



HAL
open science

A new heterogeneous asynchronous explicit–implicit time integrator for nonsmooth dynamics

Fatima-Ezzahra Fekak, Michael Brun, Anthony Gravouil, Bruno Depale

► **To cite this version:**

Fatima-Ezzahra Fekak, Michael Brun, Anthony Gravouil, Bruno Depale. A new heterogeneous asynchronous explicit–implicit time integrator for nonsmooth dynamics. *Computational Mechanics*, 2017, 60 (1), pp.1-21. 10.1007/s00466-017-1397-0 . hal-04683723

HAL Id: hal-04683723

<https://hal.science/hal-04683723v1>

Submitted on 3 Sep 2024

HAL is a multi-disciplinary open access archive for the deposit and dissemination of scientific research documents, whether they are published or not. The documents may come from teaching and research institutions in France or abroad, or from public or private research centers.

L'archive ouverte pluridisciplinaire **HAL**, est destinée au dépôt et à la diffusion de documents scientifiques de niveau recherche, publiés ou non, émanant des établissements d'enseignement et de recherche français ou étrangers, des laboratoires publics ou privés.

A new heterogeneous asynchronous explicit–implicit time integrator for nonsmooth dynamics

Fatima-Ezzahra Fekak¹ · Michael Brun² · Anthony Gravouil^{1,3} · Bruno Depale⁴

Received: ... / Accepted: ...

Abstract In computational structural dynamics, particularly in the presence of nonsmooth behavior, the choice of the time-step and the time integrator has a critical impact on the feasibility of the simulation. Furthermore, in some cases, as in the case of a bridge crane under seismic loading, multiple time-scales coexist in the same problem. In that case, the use of multi-time scale methods is suitable. Here, we propose a new explicit–implicit heterogeneous asynchronous time integrator (HATI) for nonsmooth transient dynamics with frictionless unilateral contacts and impacts. Furthermore, we present a new explicit time integrator for contact/impact problems where the contact constraints are enforced using a Lagrange multiplier method. In other words, the aim of this paper consists in using an explicit time integrator with a fine time scale in the contact area for reproducing high frequency phenomena, while an implicit time integrator is adopted in the other parts in order to reproduce much low frequency phenomena and to optimize the CPU time. In a first step, the explicit time integrator is tested on a one-dimensional example and compared to Moreau-Jean’s event-capturing schemes. The explicit algorithm is found to be very accurate and the scheme has generally a higher order of convergence than Moreau-Jean’s schemes and provides also an excellent energy behavior. Then, the two time scales explicit–implicit

HATI is applied to the numerical example of a bridge crane under seismic loading. The results are validated in comparison to a fine scale full explicit computation. The energy dissipated in the implicit–explicit interface is well controlled and the computational time is lower than a full-explicit simulation.

Keywords Contact · Impact · Nonsmooth dynamics · Explicit time integrator · Heterogeneous asynchronous time integrator · Time-stepping scheme

1 Introduction

In transient dynamics, time integration schemes for linear and nonlinear problems have been developed for a long time as well as their stability and accuracy largely studied in order to ensure convergence. For linear problems, we can adopt schemes that allow to preserve the second-order accuracy, the most popular being the implicit α -schemes (HHT- α , CH- α and WBZ- α). Some other schemes enable possible temporal discontinuities to be accounted for with high-order accuracy, such as the Time Discontinuous Galerkin (TDG) scheme. However, for nonlinear problems, the previous implicit schemes can lose their unconditional stability. Some recent works have still been devoted to study and clarify specific issues in nonlinear regime, such as accuracy, stability, high-frequency behavior, energy-decaying properties, overshoot, and numerical integration of internal forces. For this purpose, energy-conserving [9, 15, 77], symplectic (energy-momentum conserving) [60, 79] and variational [58, 67] time integrators have been proposed.

However, the main drawback of this standard approach is that the same time integrator (homogeneous) and the same time scale (synchronous) are used for all the finite elements of

✉ Fatima-Ezzahra Fekak
fatima-ezzahra.fekak@insa-lyon.fr

¹ Univ Lyon, INSA-Lyon, CNRS UMR5259, LaMCoS, 69621 Villeurbanne, France

² Univ Lyon, INSA-Lyon, EA4126, LGCIE, 69621 Villeurbanne, France

³ Institut Universitaire de France, Paris, France

⁴ Technical Center of Mechanical Industry, 52, avenue Félix Louat, 60300 Senlis, France

the mesh. This is why considerable improvements have been made to develop heterogeneous (each part of the mesh has its own time-integrator) asynchronous (each part of the mesh has its own time discretization) time integrators. It consists of dividing the considered structure into different sub-domains, individually handled by an appropriate time integrator with a chosen time step. This strategy allows to adapt the time step and the time integrator according to the specificities of the sub-domain (frequency content of the loading, presence of nonsmooth behaviors...). Engineering applications of HATI can be found for instance in multiphysics, fluid-structure interaction, safety-related impact simulations for aircraft components. The pioneer works to build HATI methods have been carried out by Belytschko, who was the first with Mullen to use a mixed explicit-implicit method [12, 13]. A detailed state of the art of HATI can be found in [44]. Here, the aim of this paper consists in using an explicit time integrator with a fine time scale in the contact area characterized by high frequency phenomena, and an implicit time integrator in the other parts reproducing much lower frequency phenomena in order to optimize the CPU time.

There are essentially two methods to link at the interface the different sub-domains. The first approach consists in linking the sub-domains using a displacement continuity condition. The second approach consists in linking the sub-domains with a velocity continuity condition. The GC method, proposed by Gravouil and Combescure [27–29, 42, 43], is built with a velocity continuity at the interface at the finest time scale. The authors showed that any Newmark time integrators can be coupled with their own time scale, providing a general demonstration of stability using the pseudo-energy method [28, 42, 50]. Many engineering applications of this method are available [18, 19, 23, 28, 29, 37, 42, 43, 64–66]. Mahjoubi, Gravouil and Combescure have developed the MGC method in order to couple the Newmark schemes, the HHT- α , Simo and Krenk schemes in linear dynamics [64–66]. Unlike the GC method, the MGC is also based on a velocity continuity but at the macro time scale. Recently, two new coupling methods, BGC-micro (Brun, Gravouil, Combescure) and BGC-macro, have been proposed [44]. The BGC-macro is a macro-time-based method as the MGC method. However, it guarantees the zero value of the interface pseudo-energy whatever is the α time integrator. The BGC-micro is micro-time-based method as the GC method. The BGC-micro method exactly matches the GC method for Newmark schemes but it can also be employed for the α -schemes (more details can be found in [44]). In this paper, we will use the GC method because only Newmark schemes are involved.

In this work, we have also been interested in nonsmooth transient dynamics including impact. Research in this domain is still very active because it has not reached the maturity of other domains yet. Applications include many fields such as the animated computer graphics [10, 46], the dynamics

of machines especially robotics [36], dynamics of structures under transient loading (earthquake, strong wind,...) [6] and granular dynamics [72].

When treating contact problems, two mechanical behaviors have to be distinguished. The first one is the contact which is a smooth behavior without any time discontinuities in velocity, force or acceleration. The second one is the impact which is a nonsmooth behavior introducing time discontinuities (velocity jumps). The enforcement of unilateral contact constraints may generate impacts which introduce time discontinuities (velocity jumps) in the balance equations. This nonsmoothness behavior requires the development of specific time integrators. They are usually classified in two categories [2, 3, 16, 71] (an other classification based on the enforcement method of the contact constraints can be found in [74]):

- Event-tracking (event-driven) time integrators: These methods account for the exact constraints at event times and between events (contact or impact). This is very accurate but requires the use of some event detection procedures [83, 85] which fail if the number of events is large or infinite (*Zeno phenomenon*). In this case, these schemes become inconsistent. Event-tracking methods usually adopt a force-acceleration formulation, so they provide to the user the contact force values. Such methods are more adapted when a few and separated events occur. Some event-tracking schemes are detailed in [1, 5].
- Event-capturing (time-stepping) time integrators: These methods consider a time-discretization of the equation of motion including the contact/impact conditions. Time-capturing methods are performed when a large number of events are expected because no accurate detection of the events is needed. All the contacts/impacts are treated in the same time step. The main event-capturing method is due to Moreau and Jean [52, 70, 71]. It is based on a velocity-impulse formulation where an impact law can be considered together with the contact constraints at the velocity level. Moreau-Jean's time-stepping schemes enjoy some convergence results [8, 53, 80, 81]. The main drawback is their low order of convergence. Traditionally, they are of order one over smooth and nonsmooth periods. Recently, some methods have been developed in [2, 76] to improve the behavior of Moreau's schemes during smooth periods.

To enforce contact/impact conditions in transient dynamics, a wide range of methods have been developed. Penalty, Lagrange multiplier and augmented Lagrangian [7, 38, 78] methods are the most commonly used. Penalty methods are widely used in finite element analysis to solve contact problems [11, 14, 22, 55, 59, 63, 68, 84]. These methods tolerate a penetration between bodies, which can be reduced with a

good choice of the penalty parameters. However, the computational time may drastically increase because the time step must be severely reduced for stability reasons [14]. Thus, the main drawback of these methods is the introduction of additional parameters for which the user must select an appropriate value depending on the application under consideration. On the other hand, Lagrange multipliers methods exactly enforce the contact constraints. However, algorithms based on these methods usually require the solution of implicit system of equations [2,20,35,82]. More details about these methods and other contact algorithms can be found in [11,59]. This paper is mainly devoted to time integration for contact dynamics with different time scales. Here, we assume a Lagrange multiplier formalism with node to node contact (see [47,49,56,73] for more general contact cases).

Recently, in solid dynamics, variational or symplectic (energy-momentum conservation) time integrators [45,62] have been formulated for contact problems [39,40,48,49,60]. The resulting algorithms are implicit and require the detection of contact events. Cirak and West proposed in [26] to relax this constraint and treat the contact at the end of the time step, but their algorithm loses its variational nature: Indeed, an energy loss or gain is observed at each contact event whereas the system is supposed to conserve energy. In order to ensure the energy balance, a small time step is then required. In order to reduce this energy drift, Rychman and Lew proposed in [75] an asynchronous variational integrator where a small time step is adopted in the area involved by the contact. Our work aims to construct an heterogeneous asynchronous explicit-implicit time integrator for contact and impact dynamics. Furthermore, in order to solve the problem in the sub-domains in which contact/impact occur, we propose a new explicit time-stepping contacts/impacts time integrator using Lagrange multipliers inspired from Cirak and West's works [26].

The paper begins in Sect. 2 by proposing a space-time weak formulation for the explicit-implicit HATI for contact/impact problems. In the same framework, a Lagrange explicit time integrator for frictionless unilateral contacts and impacts is also presented. Finally, in Sect. 3, two numerical examples are studied to illustrate the HATI and the contact/impact time integrator.

2 Explicit-implicit HATI for contact/impact problems

2.1 Strong formulation for the general case of contacting deformable bodies

In this section, we define the unilateral contact constraints between two deformable bodies B_1 and B_2 . We consider the problem depicted in Fig. 1.

In Fig. 1, Ω_α ($\alpha = 1, 2$) is the current configuration of the deformable body B_α , Γ_α is its boundary. The interface Γ_α is decomposed into three distinct regions: Γ_{u_α} , Γ_{F_α} and Γ_{C_α} , respectively, the Dirichlet, Neumann parts of Γ_α and the interface including all the possible contact points. When contact occurs, $\Gamma_C = \Gamma_{C_1} = \Gamma_{C_2}$ denotes the common contact surface. Here, the normal components refer to the master body B_1 . The contact constraints to be enforced $\forall \mathbf{X}_\alpha \in \Gamma_{C_\alpha}$ and $\forall t \in [0, T]$ are summarized for frictionless response as:

$$g_N = [(\mathbf{X}_2 + \mathbf{u}_2) - (\mathbf{X}_1 + \mathbf{u}_1)] \cdot \mathbf{n}_1 \geq 0 \quad (1a)$$

$$t_N = \boldsymbol{\sigma}_\alpha \cdot \mathbf{n}_\alpha \cdot \mathbf{n}_\alpha \leq 0, \quad \alpha = 1, 2 \quad (1b)$$

$$g_N \cdot t_N = 0 \quad (1c)$$

where $\boldsymbol{\sigma}_\alpha$ is the Cauchy stress field in Ω_α , \mathbf{u}_α is the displacement field at the point $\mathbf{X}_\alpha \in \Gamma_{C_\alpha}$, and \mathbf{n}_α is the outward normal to Γ_{C_α} . We assume small displacements and small strains.

The inequality (1a) is the impenetrability condition. It stipulates that the two solids can be either separated from each other ($g_N > 0$) or contiguous to each other ($g_N = 0$), g_N being called the gap function. The inequality (1b) is called the intensity condition [11,31]. It expresses that the two solids can be either inactive with respect to each other ($t_N = 0$) or press on each other ($t_N < 0$), t_N being the contact pressure acting at the point $\mathbf{X}_\alpha \in \Gamma_{C_\alpha}$. The Eq. (1c) is called the complementarity condition. It states that the normal component of the contact force does no work. It also describes the fact that the two solids are either distant and inactive ($g_N > 0, t_N = 0$) or contiguous and interactive ($g_N = 0, t_N < 0$). The three unilateral contact conditions (1a), (1b) and (1c) are usually called Signorini's conditions, but, as explained in [31], it seems fair to attribute them to Hertz, Signorini and Moreau. Therefore, in this paper, these conditions are called HSM conditions. Furthermore, for structural dynamics, we will use the HSM conditions rewritten in terms of velocity. The viability lemma introduced by Moreau [71] justifies the following formulation of a velocity-impulse HSM conditions as an algorithm:

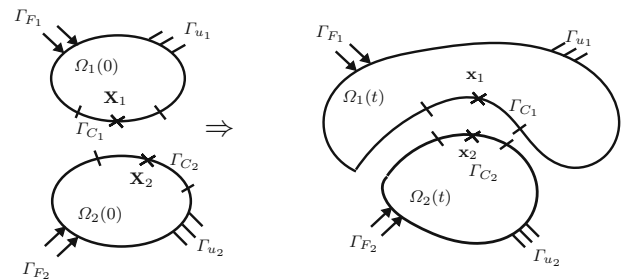


Fig. 1 Configuration of two deformable bodies in contact

$$\begin{cases} g_N \geq 0 \\ t_N \leq 0 \\ g_N \cdot t_N = 0 \end{cases} \iff \begin{cases} \text{if } g_N > 0 \text{ then } i_N = 0 \\ \text{if } g_N = 0 \text{ then } \begin{cases} \dot{g}_N \geq 0 \\ i_N \leq 0 \\ \dot{g}_N \cdot i_N = 0 \end{cases} \end{cases} \quad (2)$$

where i_N is the contact impulse and \dot{g}_N is the normal component of the relative velocity:

$$\dot{g}_N = [\dot{\mathbf{u}}_2 - \dot{\mathbf{u}}_1] \cdot \mathbf{n}_1 = [\mathbf{v}_2 - \mathbf{v}_1] \cdot \mathbf{n}_1 \quad (3)$$

with superscript dots denoting material time derivatives.

Therefore, the two contacting bodies are governed by the following momentum equation, the kinematic relations and the contact constraints:

$$\begin{cases} \operatorname{div} \boldsymbol{\sigma} + \mathbf{f}_d = \rho \dot{\mathbf{v}} & \text{in } \Omega = \Omega_1 \cup \Omega_2 \\ \boldsymbol{\sigma} \cdot \mathbf{n} = \mathbf{F}_d & \text{on } \Gamma_F = \Gamma_{F_1} \cup \Gamma_{F_2} \\ \boldsymbol{\sigma} \cdot \mathbf{n} = \mathbf{t}_N & \text{on } \Gamma_C \\ \mathbf{u} = \mathbf{u}_d & \text{on } \Gamma_u = \Gamma_{u_1} \cup \Gamma_{u_2} \\ \boldsymbol{\epsilon} = \frac{1}{2}(\nabla \mathbf{u} + (\nabla \mathbf{u})^T) & \text{in } \Omega \\ \mathbf{u}(0) = \mathbf{u}_0; \quad \mathbf{v}(0) = \mathbf{v}_0 & \text{in } \Omega \\ \text{stress-strain law (bulk material law)} & \text{in } \Omega \\ \text{HSM conditions (interface material law)} & \text{on } \Gamma_C \end{cases} \quad (4)$$

where ρ is the density and \mathbf{f}_d is the body force.

In the following, the stress strain law is assumed to be linear elastic homogeneous isotropic (or more generally based on the free energy and the pseudo-dissipation potential (see [61])). The interface material law can include unilateral contact with impact law (Newton's impact law), Coulomb's law, or more complex dissipative interface laws [33,38]. Here, we deal with only the case of unilateral frictionless contact.

2.2 Space-time weak formulation of explicit-implicit HATI for contact/impact problems

In this section, we present the space-time weak formulation for the new explicit-implicit HATI for contact/impact problems. The method used here is the multi-scale method developed by Gravouil and Combescure [27,29,42,43]. This approach allows us to consider different sub-domains with their own time scale (asynchronous) and their own time integrator (heterogeneous) (see Fig. 2). The first sub-domain Ω_E contains the contact areas where a new explicit contact/impact time integrator, developed in Sect. 2.3, is used with a suitable time step depending on the mesh. The second sub-domain Ω_I includes the remaining of the structure where the implicit Newmark average acceleration scheme is adopted.

In Fig. 2, Γ_D^E and Γ_D^I are the interfaces where Dirichlet conditions are imposed, Γ_C^E the interface including all the prospective contact points, Γ_G the interface between the two sub-domains. The indexes j and m represent, respectively, the micro-time scale of the explicit time integrator and the

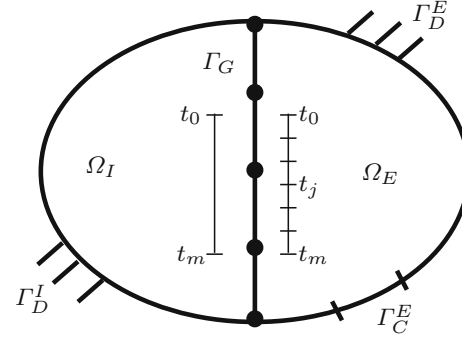


Fig. 2 Sub-domains configuration

macro-time scale of the implicit time integrator. The exponents E and I represent the quantities associated with the explicit Ω_E and the implicit Ω_I sub-domains, respectively. In this paper, we consider the finite element method for the space discretization. The spatially discretized kinematic constraints to be imposed on the interface Γ_G are introduced in terms of velocity as follows [27,29,42,43]:

$$\mathbf{L}_G^E \dot{\mathbf{U}}^E(t) + \mathbf{L}_G^I \dot{\mathbf{U}}^I(t) = 0 \quad \forall t \in [t_0, t_m] \quad (5)$$

where, \mathbf{L}_G^k ; $k = I, E$ are the connectivity matrices at the interface Γ_G , $\mathbf{U}^k(t)$ is the spatially discretized displacement field in Ω_k at time t . Single and double superposed dots over a quantity denote its first and second time derivatives, respectively.

In order to obtain the weak space-time formulation, we introduce the following action integral which is the key point for building the explicit-implicit HATI time integrator (see [44] for details):

$$\begin{aligned} \tilde{A}(\mathbf{U}^I, \dot{\mathbf{U}}^I, \mathbf{U}^E, \dot{\mathbf{U}}^E, t_c) &= A^I(\mathbf{U}^I, \dot{\mathbf{U}}^I) + \tilde{A}^E(\mathbf{U}^E, \dot{\mathbf{U}}^E, t_c) \\ &+ \int_{t_0}^{t_m} \left(\mathbf{L}_G^E \dot{\mathbf{U}}^E(t) + \mathbf{L}_G^I \dot{\mathbf{U}}^I(t) \right)^T \boldsymbol{\lambda}_G dt \end{aligned} \quad (6)$$

where $\boldsymbol{\lambda}_G$ is the Lagrange multipliers vector associated with the kinematic constraints (5) on Γ_G . It represents the generalized momentum [44], t_c is the unknown contact/impact time, A^I is the following well-know action integral associated with the sub-domain Ω_I [41]:

$$A^I(\mathbf{U}^I, \dot{\mathbf{U}}^I) = \int_{t_0}^{t_m} \mathcal{L}^I(\mathbf{U}^I(t), \dot{\mathbf{U}}^I(t)) dt \quad (7)$$

where the term \tilde{A}^E is the augmented action integral associated to the sub-domain Ω_E containing the contact boundary. For sake of simplicity, we consider that just one event (contact/impact) occurs at time t_c over the time interval $[t_0, t_m]$ as in Cirak and West [26]. The same approach can be extended

to a multi-event case. In Ω_E , we consider the following special action integral for contact problems, introduced in [26], as follows:

$$A^E(\mathbf{U}^E(t), \dot{\mathbf{U}}^E(t), t_c) = \int_{t_0}^{t_c} \mathcal{L}^E(\mathbf{U}^E(t), \dot{\mathbf{U}}^E(t)) dt + \int_{t_c}^{t_m} \mathcal{L}^E(\mathbf{U}^E(t), \dot{\mathbf{U}}^E(t)) dt \quad (8)$$

where \mathcal{L}^k ; $k = I, E$ is the spatially discretized Lagrangian of the sub-domain Ω_k :

$$\mathcal{L}^k(\mathbf{U}^k(t), \dot{\mathbf{U}}^k(t)) = \mathcal{T}^k(\dot{\mathbf{U}}^k(t)) - \mathcal{V}^k(\mathbf{U}^k(t)) \quad (9)$$

The spatially discretized Lagrangian \mathcal{L}^k is the difference between the kinetic energy \mathcal{T}^k and the potential energy \mathcal{V}^k , given by:

$$\mathcal{T}(\dot{\mathbf{U}}^k(t)) = \frac{1}{2} \dot{\mathbf{U}}^k(t)^T \mathbf{M}^k \dot{\mathbf{U}}^k(t) \quad (10)$$

$$\begin{aligned} \mathcal{V}(\mathbf{U}^k(t)) &= \mathcal{V}_{int}^k(\mathbf{U}^k(t)) - \mathcal{V}_{ext}^k(\mathbf{U}^k(t)) \\ &= (\mathbf{F}_{int}^k)^T \mathbf{U}^k - (\mathbf{F}_{ext}^k)^T \mathbf{U}^k \end{aligned} \quad (11)$$

where \mathbf{M}^k is the symmetric definite-positive mass matrix of the sub-domain Ω_k , \mathcal{V}_{int}^k and \mathcal{V}_{ext}^k are, respectively the internal and external potential energies, \mathbf{F}_{int}^k denote the internal forces and \mathbf{F}_{ext}^k the external forces.

In presence of contact, the admissible set of p points is:

$$C(t) = \{\mathbf{x} \in \partial\Omega_E \mid g_N^l(t) \geq 0; \forall l \in \{1, \dots, p\}\} \quad (12)$$

The boundary ∂C , given by $g_N^l(t_c) = 0; \forall l \in \{1, \dots, p\}$, is the set of points where the contact has just occurred. Note that the (non-unit) normal to ∂C is given by $\nabla \mathbf{g}_N$. In order to take into account the contact constraint $g_N^l(t_c) = 0; \forall l \in \{1, \dots, p\}$, we consider the augmented action integral:

$$\tilde{A}^E(\mathbf{U}^E, \dot{\mathbf{U}}^E, t_c) = A^E(\mathbf{U}^E, \dot{\mathbf{U}}^E) + \lambda_c^T(t_c) \mathbf{g}_N(t_c) \quad (13)$$

where λ_c is the Lagrange multiplier vector of dimension p on ∂C , verifying the following conditions:

$$\begin{cases} g_N^l(t) \geq 0 \\ \lambda_c^l(t) \geq 0 \\ \lambda_c^l(t) g_N^l(t) = 0 \end{cases} \quad \forall l \in \{1, \dots, p\}, \forall t \in [t_0, t_f] \quad (14)$$

The set of equations (14) is often called the Karush-Kuhn-Tucker conditions (KKT). We can notice here the strong link between KKT and HSM conditions given in (2).

At the equilibrium configuration, the action integral \tilde{A} is required to be stationary. Applying variational calculus as in Cirak and West [26] and Gravouil et al. [44], the space-time

weak formulation for explicit-implicit HATI time integrator for contact/impact problems can be written as follows:

$$\begin{aligned} \delta \tilde{A} &= \int_{t_0}^{t_m} \left(\frac{\partial \mathcal{L}^I}{\partial \mathbf{U}^I} - \frac{d}{dt} \left(\frac{\partial \mathcal{L}^I}{\partial \dot{\mathbf{U}}^I} \right) + ((\mathbf{L}_G^I)^T \Lambda_G)^T \right) \delta \mathbf{U}^I dt \\ &+ \int_{[t_0, t_c] \cup [t_c, t_m]} \left(\frac{\partial \mathcal{L}^E}{\partial \mathbf{U}^E} - \frac{d}{dt} \left(\frac{\partial \mathcal{L}^E}{\partial \dot{\mathbf{U}}^E} \right) + ((\mathbf{L}_G^E)^T \Lambda_G)^T \right) \delta \mathbf{U}^E dt \\ &- \left(\left[\frac{\partial \mathcal{L}^E}{\partial \dot{\mathbf{U}}^E} \right]_{t_c^-}^{t_c^+} - \lambda_c^T(t_c) \nabla \mathbf{g}_N(t_c) \right) \delta \mathbf{U}^E(t_c) \\ &- \left(\left[\mathcal{L}^E \right]_{t_c^-}^{t_c^+} - \lambda_c^T(t_c) \nabla \mathbf{g}_N(t_c) \dot{\mathbf{U}}^E(t_c) \right) \delta t_c \\ &+ \delta \lambda_c^T(t_c) \mathbf{g}_N(t_c) + \int_{t_0}^{t_m} \left(\mathbf{L}_G^E \dot{\mathbf{U}}^E(t) + \mathbf{L}_G^I \dot{\mathbf{U}}^I(t) \right)^T \delta \lambda_G dt \\ &= 0 \quad \forall \delta \mathbf{U}^k \in \mathcal{U}^0, \delta t_c \in \mathcal{I}_c^0, \delta \lambda_c \in \Lambda_c^0, \delta \lambda_G \in \Lambda_G^0 \end{aligned} \quad (15)$$

where $(\mathbf{L}_G^k)^T \Lambda_G$ ($k = I, E$) represent the interface forces. As shown in [44], we have the relationship $\Lambda_G = -\dot{\lambda}_G$, t_c^- and t_c^+ are, respectively, instants just before and after contact/impact event. The spaces of the test functions \mathcal{U}^0 , \mathcal{I}_c^0 , Λ_c^0 , and Λ_G^0 , introduced in (15), are [44, 82]:

$$\begin{aligned} \mathcal{U}^0 &= \{\delta \mathbf{U}^k \in H^1(\Omega_k \times [t_0, t_m]) \mid \delta \mathbf{U}^k = 0 \text{ on } \Gamma_{ik}, \\ &\delta \mathbf{U}^k(t_0) = 0, \delta \mathbf{U}^k(t_m) = 0 \text{ in } \Omega_k\} \end{aligned} \quad (16)$$

$$\Lambda_c^0 = \{\delta \lambda_c \in H^{-\frac{1}{2}}(\partial C \times [t_0, t_m]) \mid \delta \lambda_c^l \geq 0; l \in \{1, \dots, p\}\} \quad (17)$$

$$\Lambda_G^0 = \{\delta \lambda_G \in H^1(\Gamma_G \times [t_0, t_m])\} \quad (18)$$

$$\mathcal{I}_c^0 = [t_0, t_m] \quad (19)$$

where H^1 and $H^{-\frac{1}{2}}$ are Hilbert spaces with suitable properties of regularity.

From (15), we obtain the following equations:

– In Ω_I :

$$\frac{\partial \mathcal{L}^I}{\partial \mathbf{U}^I} - \frac{d}{dt} \left(\frac{\partial \mathcal{L}^I}{\partial \dot{\mathbf{U}}^I} \right) + ((\mathbf{L}_G^I)^T \Lambda_G)^T = 0 \quad \forall t \in [t_0, t_m] \quad (20)$$

– In Ω_E :

$$\begin{cases} \frac{\partial \mathcal{L}^E}{\partial \mathbf{U}^E} - \frac{d}{dt} \left(\frac{\partial \mathcal{L}^E}{\partial \dot{\mathbf{U}}^E} \right) + ((\mathbf{L}_G^E)^T \Lambda_G)^T = 0 & \forall t \in [t_0, t_c^-] \cup [t_c^+, t_m] \\ \left[\frac{\partial \mathcal{L}^E}{\partial \dot{\mathbf{U}}^E} \right]_{t_c^-}^{t_c^+} = \lambda_c^T(t_c) \nabla \mathbf{g}_N(t_c) \\ \left[\mathcal{L}^E \right]_{t_c^-}^{t_c^+} - \left[\frac{\partial \mathcal{L}^E}{\partial \dot{\mathbf{U}}^E} \right]_{t_c^-}^{t_c^+} \dot{\mathbf{U}}^E(t_c) = 0 \\ g_N^l(t_c) = 0; \quad \forall l \in \{1, \dots, p\} \end{cases} \quad (21)$$

– On Γ_G :

$$\mathbf{L}_G^E \dot{\mathbf{U}}^E(t) + \mathbf{L}_G^I \dot{\mathbf{U}}^I(t) = 0 \quad \forall t \in [t_0, t_m] \quad (22)$$

Replacing the Lagrangian \mathcal{L}^k with its expression (9) in (21) and (20), we obtain the following spatially discretized equilibrium system of each sub-domain:

– In Ω_I :

$$\mathbf{M}^I \ddot{\mathbf{U}}^I(t) + \mathbf{F}_{int}^I(t) = \mathbf{F}_{ext}^I(t) + \mathbf{F}_{link}^I(t) \quad \forall t \in [t_0, t_m] \quad (23)$$

– In Ω_E :

$$\mathbf{M}^E \ddot{\mathbf{U}}^E(t) + \mathbf{F}_{int}^E(t) = \mathbf{F}_{ext}^E(t) + \mathbf{F}_{link}^E(t) \quad \forall t \in [t_0, t_c^-] \cup [t_c^+, t_f] \quad (24a)$$

$$\left[\mathbf{M}^E \dot{\mathbf{U}}^E(t) \right]_{t_c^-}^{t_c^+} = \nabla \mathbf{g}_N^T(t_c) \lambda_c(t_c) = i_N \mathbf{n}_1 \quad (24b)$$

$$\left[(\mathbf{M}^E \dot{\mathbf{U}}^E(t))^T (\mathbf{M}^E)^{-1} (\mathbf{M}^E \dot{\mathbf{U}}^E(t)) \right]_{t_c^-}^{t_c^+} = 0 \quad (24c)$$

$$g_N^l(t_c) = 0; \quad \forall l \in \{1, \dots, p\} \quad (24d)$$

where $\mathbf{F}_{link}^k = (\mathbf{L}_G^k)^T \Lambda_G$ are the connecting forces at the interface Γ_G , (23) represents the classical equilibrium equation including interface forces \mathbf{F}_{link}^I which enable the sub-domains to be glued between each others, (24a) is the smooth equilibrium equation without impact completed with (24b) representing the velocity jump during impact, (24c) denotes the kinetic energy conservation during the impact. Here, we obtain the physical meaning of the Lagrange multipliers introduced in the augmented action integral (13): λ_c^l ; $l \in \{1, \dots, p\}$ represents the contact impulse i_N . We add to the set of equations (24) the KKT conditions (14) which are equivalent to the HSM conditions (2) (see Moreau [71]). Using the relation (24b), we can express the HSM conditions as follows, $\forall t \in [t_0, t_m]$, $\forall l \in \{1, \dots, p\}$:

$$\text{if } g_N^l(t) > 0 \text{ then } \lambda_c^l(t) = 0 \quad (25a)$$

$$\text{if } g_N^l(t) = 0 \text{ then } \begin{cases} \dot{g}_N^l(t) \geq 0 \\ \lambda_c^l(t) \geq 0 \\ \lambda_c^l(t) \dot{g}_N^l(t) = 0 \end{cases} \quad (25b)$$

In the next section, we focus on the problem of the sub-domain Ω_E , in which we will propose a new explicit time-integrator using Lagrange multipliers for contact/impact problems.

2.3 Explicit time integrator for contact/impact problems

Since we only deal with the sub-domain Ω_E in this section, we will remove the index E for a clearer and more general notation. Moreover, the link forces \mathbf{F}_{link}^E , enabling the gluing between sub-domains through the interface Γ_G , are omitted in this section.

2.3.1 Nonsmooth transient dynamic equation

In the following, we use the theory of nonsmooth dynamics [70]. It allows us to write the smooth dynamics evolution (24a) and the nonsmooth impact equation (24b) in a single balance equation. In this framework, the differential measure of the velocity is decomposed into a smooth and a nonsmooth parts. This technique has been used and developed in [4, 17, 24, 25, 76] :

$$d\dot{\mathbf{U}} = d\dot{\mathbf{U}}_s + d\dot{\mathbf{U}}_{ns} \quad (26)$$

where, the index s denotes a smooth quantity and the index ns denotes a nonsmooth quantity.

In smooth dynamics, $\dot{\mathbf{U}}_s$ is at least continuous, therefore the acceleration $\ddot{\mathbf{U}}$ has a finite value. Then, we can write:

$$d\dot{\mathbf{U}}_s = \ddot{\mathbf{U}} dt \quad (27)$$

For the nonsmooth part, we have to express the velocity jump:

$$d\dot{\mathbf{U}}_{ns} = \dot{\mathbf{U}}(t_c^+) - \dot{\mathbf{U}}(t_c^-) \quad (28)$$

Then, from (26), (27) and (28), we can write:

$$\mathbf{M} d\dot{\mathbf{U}} = \mathbf{M} \ddot{\mathbf{U}} dt + \mathbf{M} \left(\dot{\mathbf{U}}(t_c^+) - \dot{\mathbf{U}}(t_c^-) \right) \quad (29)$$

From (24a), we have:

$$\mathbf{M} \ddot{\mathbf{U}} dt = \mathbf{F}_{ext} dt - \mathbf{F}_{int} dt \quad (30)$$

with (24b):

$$\mathbf{M} \left(\dot{\mathbf{U}}(t_c^+) - \dot{\mathbf{U}}(t_c^-) \right) = \nabla \mathbf{g}_N^T(t_c) \lambda_c(t_c) \quad (31)$$

Substituting (30) and (31) into (29) gives:

$$\mathbf{M} d\dot{\mathbf{U}}(t) + \mathbf{F}_{int}(t) dt = \mathbf{F}_{ext}(t) dt + d\mathbf{I}(t) \quad \forall t \in [t_0, t_m] \quad (32)$$

where the impact impulse is expressed as:

$$d\mathbf{I}(t) = \begin{cases} 0 & \forall t \in [t_0, t_c^-] \cup [t_c^+, t_m] \\ \nabla \mathbf{g}_N^T(t_c) \lambda_c(t_c) & \end{cases} \quad (33)$$

In addition to the nonsmooth transient dynamic equation (32), we have the HSM requirements (25). Finally, the spatially discretized Lagrange multiplier form of the impact/contact problem can be written as follows:

$$\begin{cases} \mathbf{M}d\dot{\mathbf{U}} + \mathbf{F}_{int}dt = \mathbf{F}_{ext}dt + d\mathbf{I} \\ d\mathbf{I} = \mathbf{L}_c^T d\lambda_c \quad (\mathbf{L}_c = \nabla \mathbf{g}_N) \\ \mathbf{v}_c = \mathbf{L}_c \dot{\mathbf{U}} = \dot{\mathbf{g}}_N \\ \left\{ \begin{array}{l} \text{if } g_N^l > 0 \text{ then } \lambda_c^l = 0 \\ \text{if } g_N^l = 0 \text{ then } \begin{cases} v_c^l \geq 0 \\ \lambda_c^l \geq 0 \\ v_c^l \lambda_c^l = 0 \end{cases} \end{array} \right. \quad \forall l \in \{1, \dots, p\} \end{cases} \quad (34)$$

where \mathbf{L}_c^T is a prolongation operator from Γ_C^E to Ω_E , \mathbf{L}_c a restriction operator from Ω_E to Γ_C^E and \mathbf{v}_c the local velocity associated with contact points.

Remark The set of equations (34) remains valid for rigid body systems, but unlike the deformable body systems, an impact law has to be considered because the HSM conditions do not give enough information (see [52]). The impact law could be, for instance, the Newton restitution law: $\mathbf{v}_c(t_c^+) = -e\mathbf{v}_c(t_c^-)$, where e is the coefficient of restitution. As mentioned in [52], the HSM conditions (25) correspond to a coefficient of restitution $e = 0$. Since this paper is mainly devoted to deformable bodies, impact laws will not be discussed in the following.

In the next part, we propose a time-discretization based on an original explicit approach for nonsmooth dynamics with Lagrange multipliers.

2.3.2 Time discretization based on an explicit approach for contact dynamics

For the time discretization, we consider the following semi-discretized equilibrium nonsmooth equation obtained from the previous developments:

$$\mathbf{M}d\dot{\mathbf{U}} + (\mathbf{F}_{int} + \mathbf{C}\dot{\mathbf{U}})dt = \mathbf{F}_{ext}dt + d\mathbf{I} \quad (35)$$

where we have introduced the possible damping matrix \mathbf{C} . In the following, we will employ the well-known Central Difference time integrator (CD) (see [11, 41]) in order to proceed to the time discretization. Indeed, the CD time integrator is symplectic for conservative mechanical systems and therefore preserves energy, linear and angular momentum [54]. Here, we consider an explicit velocity approach [11, 41]. Furthermore, based on the explicit mid-point time discretization (see for instance Casadei [21]), we consider the time interval $[t_{n+\frac{1}{2}}, t_{n+\frac{3}{2}}]$. Integrating both sides of the equation (35) over the time step $[t_{n+\frac{1}{2}}, t_{n+\frac{3}{2}}]$ of length Δt gives:

$$\begin{aligned} & \int_{n+\frac{1}{2}}^{n+\frac{3}{2}} \mathbf{M}d\dot{\mathbf{U}} + \int_{n+\frac{1}{2}}^{n+\frac{3}{2}} \mathbf{F}_{int} dt + \int_{n+\frac{1}{2}}^{n+\frac{3}{2}} \mathbf{C}\dot{\mathbf{U}} dt \\ & = \int_{n+\frac{1}{2}}^{n+\frac{3}{2}} \mathbf{F}_{ext} dt + \int_{n+\frac{1}{2}}^{n+\frac{3}{2}} d\mathbf{I} \end{aligned} \quad (36)$$

From the previous time weak form (36), the discretized non-smooth equilibrium equation can be written as follows:

$$\begin{aligned} \mathbf{M}_{lump}(\dot{\mathbf{U}}_{n+\frac{3}{2}} - \dot{\mathbf{U}}_{n+\frac{1}{2}}) + \mathbf{F}_{int,n+1}(\mathbf{U}_{n+1})\Delta t + \mathbf{C}\dot{\mathbf{U}}_{n+\frac{1}{2}}\Delta t \\ = \mathbf{F}_{ext,n+1}\Delta t + \mathbf{I}_{n+1} \end{aligned} \quad (37)$$

with a damping contribution written at $t_{n+\frac{1}{2}}$ in order to ensure a fully explicit approach (see Belytschko [11]), \mathbf{M}_{lump} is the lumped mass matrix [11, 41, 86], $\dot{\mathbf{U}}_{n+\frac{3}{2}}$ and $\dot{\mathbf{U}}_{n+\frac{1}{2}}$ are, respectively, the velocity vectors at time $t_{n+\frac{3}{2}}$ and $t_{n+\frac{1}{2}}$, \mathbf{U}_{n+1} , $\mathbf{F}_{int,n+1}$ and $\mathbf{F}_{ext,n+1}$ are, respectively, the displacement, the internal and the external forces at time t_{n+1} , \mathbf{I}_{n+1} is the contact/impact impulse at time t_{n+1} .

For numerical implementation, (37) is rewritten as follows (all the known terms are put on the right hand side):

$$\begin{aligned} \mathbf{M}_{lump}\dot{\mathbf{U}}_{n+\frac{3}{2}} = \mathbf{M}_{lump}\dot{\mathbf{U}}_{n+\frac{1}{2}} \\ + \Delta t (\mathbf{F}_{ext,n+1} - \mathbf{F}_{int,n+1} - \mathbf{C}\dot{\mathbf{U}}_{n+\frac{1}{2}}) \\ + \mathbf{I}_{n+1} \end{aligned} \quad (38)$$

Let's now introduce the smooth acceleration $\ddot{\mathbf{U}}_s$, the non-smooth velocity $\dot{\mathbf{U}}_I$ coming from the impact impulse defined in (33) and \mathbf{W} the velocity like quantity including both previous contributions:

$$\ddot{\mathbf{U}}_{s,n+1} = \mathbf{M}_{lump}^{-1} (\mathbf{F}_{ext,n+1} - \mathbf{F}_{int,n+1} - \mathbf{C}\dot{\mathbf{U}}_{n+\frac{1}{2}}) \quad (39)$$

$$\dot{\mathbf{U}}_{I,n+1} = \mathbf{M}_{lump}^{-1} \mathbf{I}_{n+1} \quad (40)$$

$$\mathbf{W}_{n+1} = \Delta t \ddot{\mathbf{U}}_{s,n+1} + \dot{\mathbf{U}}_{I,n+1} \quad (41)$$

Substituting (39), (40) and (41) into (38), the equilibrium equation (37) can be rewritten as:

$$\begin{aligned} \dot{\mathbf{U}}_{n+\frac{3}{2}} = \dot{\mathbf{U}}_{n+\frac{1}{2}} + \Delta t \ddot{\mathbf{U}}_{s,n+1} + \dot{\mathbf{U}}_{I,n+1} \\ = \dot{\mathbf{U}}_{n+\frac{1}{2}} + \mathbf{W}_{n+1} \end{aligned} \quad (42)$$

Then the displacement and velocity at time t_{n+1} are obtained through the explicit CD approximation formulae [11, 41, 57], by distinguishing smooth and non-smooth parts as follows (see Eq. (26) and Acary [4] for a similar smooth/nonsmooth decomposition):

$$\begin{aligned} \mathbf{U}_{n+1} = (\mathbf{U}_n + \Delta t \dot{\mathbf{U}}_n + \frac{\Delta t^2}{2} \ddot{\mathbf{U}}_{s,n}) + (\frac{\Delta t}{2} \dot{\mathbf{U}}_{I,n}) \\ = \mathbf{U}_{s,n+1} + \mathbf{U}_{ns,n+1} \end{aligned} \quad (43a)$$

$$\begin{aligned} \dot{\mathbf{U}}_{n+1} = (\dot{\mathbf{U}}_n + \frac{\Delta t}{2} (\ddot{\mathbf{U}}_{s,n+1} + \ddot{\mathbf{U}}_{s,n})) + (\frac{1}{2} (\dot{\mathbf{U}}_{I,n+1} + \dot{\mathbf{U}}_{I,n})) \\ = \dot{\mathbf{U}}_{s,n+1} + \dot{\mathbf{U}}_{ns,n+1} \end{aligned} \quad (43b)$$

Finally, introducing (41) in (43), one obtains:

$$\mathbf{U}_{n+1} = \mathbf{U}_n + \Delta t \dot{\mathbf{U}}_n + \frac{\Delta t}{2} \mathbf{W}_n \quad (44a)$$

$$\dot{\mathbf{U}}_{n+1} = \dot{\mathbf{U}}_n + \frac{1}{2} (\mathbf{W}_{n+1} + \mathbf{W}_n) \quad (44b)$$

In practice, the expressions (44a) and (44b) are useful to establish the discrete form of the energy balance equation (see ‘‘Appendix 2.1’’).

As explained in Sect. 1, the contact is a smooth interface behavior (contrary to impact which is nonsmooth). Then, when contact occurs, the contact force and the acceleration have finite values and can be calculated as follows:

$$\mathbf{F}_{c,n+1} = \frac{\mathbf{I}_{n+1}}{\Delta t} \quad (45)$$

and [11,41]:

$$\ddot{\mathbf{U}}_{n+1} = \frac{\dot{\mathbf{U}}_{n+\frac{3}{2}} - \dot{\mathbf{U}}_{n+\frac{1}{2}}}{\Delta t} = \frac{\mathbf{W}_{n+1}}{\Delta t} \quad (46)$$

Finally, the new explicit time integrator using Lagrange multipliers for a contact/impact problem is summarized as follows:

$$\begin{cases} \mathbf{U}_{n+1} = \mathbf{U}_n + \Delta t \dot{\mathbf{U}}_n + \frac{\Delta t}{2} \mathbf{W}_n \\ \mathbf{g}_{N,n+1} = \mathbf{L}_{c,n+1} \mathbf{U}_{n+1} \\ \mathbf{W}_{n+1} = \mathbf{M}_{lump}^{-1} [\Delta t (\mathbf{F}_{ext,n+1} - \mathbf{F}_{int,n+1} - \mathbf{C} \dot{\mathbf{U}}_{n+\frac{1}{2}}) + \mathbf{I}_{n+1}] \\ \dot{\mathbf{U}}_{n+\frac{3}{2}} = \dot{\mathbf{U}}_{n+\frac{1}{2}} + \mathbf{W}_{n+1} \\ \mathbf{v}_{c,n+\frac{3}{2}} = \mathbf{L}_{c,n+1} \dot{\mathbf{U}}_{n+\frac{3}{2}} \\ \mathbf{I}_{n+1} = \mathbf{L}_{c,n+1}^T \boldsymbol{\lambda}_{c,n+\frac{3}{2}} \\ \begin{cases} \text{if } g_{N,n+1}^l > 0 \text{ then } \lambda_{c,n+\frac{3}{2}}^l = 0 \\ \text{if } g_{N,n+1}^l \leq 0 \text{ then } \begin{cases} v_{c,n+\frac{3}{2}}^l \geq 0 \\ \lambda_{c,n+\frac{3}{2}}^l \geq 0 \\ v_{c,n+\frac{3}{2}}^l \lambda_{c,n+\frac{3}{2}}^l = 0 \end{cases} \end{cases} \quad \forall l \in \{1, \dots, p\} \end{cases} \end{cases} \quad (47)$$

where the state vector is $(\mathbf{U}_{n+1}, \dot{\mathbf{U}}_{n+\frac{3}{2}}, \mathbf{W}_{n+1})$.

Remark Here we can notice that due to the time-discretization, we have slightly modified the HSM conditions (25b). Indeed, in order to build a time-stepping algorithm, we allow an interpenetration ($g_{N,n+1}^l \leq 0$) at the discrete time.

Multiplying the nonsmooth equilibrium equation (38) by $\mathbf{L}_{n+1} \mathbf{M}_{lump}^{-1}$ gives the local impact/contact equation to be solved:

$$\mathbf{H} \boldsymbol{\lambda}_{c,n+\frac{3}{2}} = \mathbf{v}_{c,n+\frac{3}{2}} - \mathbf{L}_{c,n+1} (\dot{\mathbf{U}}_{n+\frac{1}{2}} + \Delta t \mathbf{M}_{lump}^{-1} (\mathbf{F}_{ext,n+1} - \mathbf{F}_{int,n+1} - \mathbf{C} \dot{\mathbf{U}}_{n+\frac{1}{2}})) \quad (48)$$

where

$$\mathbf{H} = \mathbf{L}_{c,n+1} \mathbf{M}_{lump}^{-1} \mathbf{L}_{c,n+1}^T \quad (49)$$

It is important to note that the Steklov-Poincaré (or Delassus) operator \mathbf{H} is diagonal because we assume matching meshes and \mathbf{M}_{lump}^{-1} is diagonal. However, if \mathbf{H} is not diagonal, a system solver is then required. Moreover, when assuming $e = 0$ (see remark above), the local relative velocity at contact points $\mathbf{v}_{c,n+\frac{3}{2}} = 0$.

The set of equations (47) and (48) is the basis for a general explicit formulation with Lagrange multipliers for contact/impact dynamics. The implementation of this time integrator is illustrated in ‘‘Appendix 1’’. The corresponding discrete energy balance equation is also given in ‘‘Appendix 2.1’’. In the following, this algorithm is called CD-Lagrange time integrator. It will be performed in the sub-domain Ω_E , whereas an implicit Newmark scheme will be used in the sub-domain Ω_I .

2.3.3 Moreau-Jean scheme for contact/impact problem

In order to compare the CD-Lagrange time integrator to the Moreau-Jean time integrator, the governing equations of the Moreau-Jean algorithm are reminded in the case of deformable structures. More details concerning this method can be found in [2,3,5].

The Moreau-Jean time integrator is performed using the θ method ($\theta \in [0, 1]$). On an interval $[t_n, t_{n+1}]$ of size Δt , the scheme can be summarized as follows :

$$\begin{cases} \dot{\mathbf{U}}_{n+1} = \dot{\mathbf{U}}_{free} + \hat{\mathbf{M}}^{-1} \mathbf{I}_{n+1} \\ \mathbf{U}_{n+1} = \mathbf{U}_n + \Delta t (\theta \dot{\mathbf{U}}_{n+1} + (1-\theta) \dot{\mathbf{U}}_n) \\ \mathbf{v}_{n+1} = \mathbf{L}_{n+1} \dot{\mathbf{U}}_{n+1} \\ \mathbf{I}_{n+1} = \mathbf{L}_{n+1}^T \boldsymbol{\lambda}_{n+1} \\ \begin{cases} \text{if } g_N^l(\tilde{\mathbf{x}}_{n+1}) > 0 \text{ then } \lambda_{n+1}^l = 0 \\ \text{if } g_N^l(\tilde{\mathbf{x}}_{n+1}) \leq 0 \text{ then} \\ \begin{cases} v_{n+1}^l \geq 0 \\ \lambda_{n+1}^l \geq 0 \\ v_{n+1}^l \lambda_{n+1}^l = 0 \end{cases} \end{cases} \quad \forall l \in \{1, \dots, p\} \end{cases} \end{cases} \quad (50)$$

If we assume linear elasticity ($\mathbf{F}_{int} = \mathbf{K} \mathbf{U}$ where \mathbf{K} is the global stiffness matrix), we have:

$$\hat{\mathbf{M}} = \mathbf{M} + \Delta t \theta \mathbf{C} + \Delta t^2 \theta^2 \mathbf{K} \quad (51)$$

$$\begin{aligned} \dot{\mathbf{U}}_{free} = & \dot{\mathbf{U}}_n + \Delta t \hat{\mathbf{M}}^{-1} \left(-\mathbf{C} \dot{\mathbf{U}}_n - \mathbf{K} \mathbf{U}_n - \Delta t \theta \mathbf{K} \dot{\mathbf{U}}_n \right. \\ & \left. + (\theta \mathbf{F}_{ext,n+1} + (1-\theta) \mathbf{F}_{ext,n}) \right) \end{aligned} \quad (52)$$

$\tilde{\mathbf{x}}_{n+1}$ is a prediction of the position that manages the activation of the constraints. Several formulae for this prediction are discussed in [3]. In the following, we consider:

$$\tilde{\mathbf{x}}_{n+1} = \mathbf{X}_0 + \left(\mathbf{U}_n + \frac{\Delta t}{2} \dot{\mathbf{U}}_n \right) \quad (53)$$

2.4 Time-discretization of explicit–implicit HATI for contact/impact problems

2.4.1 The governing space-time discrete equations

Let ΔT be the coarse time step and Δt the fine time step associated, respectively, with the implicit sub-domain Ω_I and the explicit one Ω_E (with possible unilateral contact and impact). We take $\Delta T = m\Delta t$ (see Fig. 2). We recall that the indexes j and m represent, respectively, the micro-time scale of the explicit time integrator and the macro-time scale of the implicit time integrator (see Fig. 2). From (22), (23), (38) and (47), we obtain the following governing equations, discretized in time and space, of the explicit–implicit HATI for contact/impact problems:

- Balance equation of each sub-domain:

$$\begin{aligned} \mathbf{M}^I \ddot{\mathbf{U}}_{n+m}^I + \mathbf{C}^I \dot{\mathbf{U}}_{n+m}^I + \mathbf{F}_{int,n+m}^I \\ = \mathbf{F}_{ext,n+m}^I + \mathbf{F}_{D,n+m}^I + \mathbf{F}_{link,n+m}^I \end{aligned} \quad (54)$$

$$\begin{aligned} \mathbf{M}_{lump}^E \dot{\mathbf{U}}_{n+j+\frac{1}{2}}^E \\ = \mathbf{M}_{lump}^E \dot{\mathbf{U}}_{n+j-\frac{1}{2}}^E - \Delta t (\mathbf{F}_{int,n+j}^E + \mathbf{C}^E \dot{\mathbf{U}}_{n+j-\frac{1}{2}}^E) \\ + \Delta t (\mathbf{F}_{ext,n+j}^E + \mathbf{F}_{D,n+j}^E + \mathbf{F}_{link,n+j}^E) + \mathbf{I}_{n+j} \end{aligned} \quad (55)$$

where we have introduced, for a more general case, the possible damping matrices \mathbf{C}^k and the forces \mathbf{F}_D^k due to possible Dirichlet conditions $\mathbf{F}_D^k = (\mathbf{L}_D^I)^T \mathbf{A}_D^k$ where \mathbf{L}_D^k are the connectivity matrices at the interface Γ_D^k . \mathbf{A} are the Lagrange multiplier vectors. In the following, we assume linear elasticity in the implicit subomain ($\mathbf{F}_{int}^I = \mathbf{K}^I \mathbf{U}^I$ where \mathbf{K}^I is the global stiffness matrix).

- Unilateral frictionless contact/impact conditions at the fine time on the interface Γ_C^E :

$$\left\{ \begin{array}{l} \mathbf{v}_{c,n+j+\frac{1}{2}} = \mathbf{L}_{c,n+j} \dot{\mathbf{U}}_{n+j+\frac{1}{2}}^E \\ \mathbf{I}_{n+j} = \mathbf{L}_{c,n+j}^T \boldsymbol{\lambda}_{c,n+j+\frac{1}{2}} \\ \mathbf{g}_{N,n+j} = \mathbf{L}_{c,n+j} \mathbf{U}_{n+j}^E \\ \left\{ \begin{array}{l} \text{if } g_{N,n+j}^I > 0 \text{ then } \lambda_{c,n+j+\frac{1}{2}}^I = 0 \\ \text{if } g_{N,n+j}^I \leq 0 \text{ then} \\ \left\{ \begin{array}{l} v_{c,n+j+\frac{1}{2}}^I \geq 0 \\ \lambda_{c,n+j+\frac{1}{2}}^I \geq 0 \\ v_{c,n+j+\frac{1}{2}}^I \lambda_{c,n+j+\frac{1}{2}}^I = 0 \end{array} \right. \end{array} \right. \quad \forall I \in \{1, \dots, p\} \end{array} \right. \quad (56)$$

The algorithm solving the contact/impact problem has been explained in the previous section.

- Dirichlet boundary conditions in each sub-domain:

$$L_D^E \dot{\mathbf{U}}_{n+j}^E = 0 \quad (57)$$

$$L_D^I \dot{\mathbf{U}}_{n+m}^I = 0 \quad (58)$$

- Velocity continuity on the interface Γ_G at the fine time t_{n+j} [42]:

$$\mathbf{L}_G^E \dot{\mathbf{U}}_{n+j}^E + \mathbf{L}_G^I \dot{\mathbf{U}}_{n+j}^I = 0 \quad (59)$$

where $\dot{\mathbf{U}}_{n+j}^I$ is the linear interpolation of $\dot{\mathbf{U}}_{n+m}^I$ at time t_{n+j} (see Eq. (74) below).

2.5 Sub-domains coupling strategy

In order to solve the interface equation (59), we split the equilibrium equation in each sub-domain into a free and a link problem, which leads to a decomposition of the velocity and displacement as follows:

$$\dot{\mathbf{U}}^k = \dot{\mathbf{U}}_{free}^k + \dot{\mathbf{U}}_{link}^k \quad (60a)$$

$$\mathbf{U}^k = \mathbf{U}_{free}^k + \mathbf{U}_{link}^k \quad (60b)$$

where the free part corresponds to the problem without any interface constraint (59) on Γ_G , and the link part is due to the interface loads \mathbf{F}_{link}^k .

In the implicit sub-domain, the use of the Newmark formulae to approximate the velocity and displacement gives:

$$\dot{\mathbf{U}}_{free,n+m}^I = {}^P \dot{\mathbf{U}}_n^I + \Delta T \gamma_I \ddot{\mathbf{U}}_{free,n+m}^I \quad (61a)$$

$$\dot{\mathbf{U}}_{link,n+m}^I = \Delta T \gamma_I \ddot{\mathbf{U}}_{link,n+m}^I \quad (61b)$$

and

$$\mathbf{U}_{free,n+m}^I = {}^P \mathbf{U}_n^I + \Delta T^2 \beta_I \ddot{\mathbf{U}}_{free,n+m}^I \quad (62a)$$

$$\mathbf{U}_{link,n+m}^I = \Delta T^2 \beta_I \ddot{\mathbf{U}}_{link,n+m}^I \quad (62b)$$

where the predictor quantities are expressed as:

$${}^P \dot{\mathbf{U}}_n^I = \dot{\mathbf{U}}_n^I + \Delta T (1 - \gamma_I) \ddot{\mathbf{U}}_n^I \quad (63a)$$

$${}^P \mathbf{U}_n^I = \mathbf{U}_n^I + \Delta T \dot{\mathbf{U}}_n^I + \frac{\Delta T^2}{2} (1 - 2\beta_I) \ddot{\mathbf{U}}_n^I \quad (63b)$$

The equations of motion are split in two parts:

$$\tilde{\mathbf{M}}^I \ddot{\mathbf{U}}_{free,n+m}^I = \mathbf{F}_{ext,n+m}^I - \mathbf{C}^I {}^P \dot{\mathbf{U}}_n^I - \mathbf{K}^I {}^P \mathbf{U}_n^I \quad (64a)$$

$$\tilde{\mathbf{M}}^I \ddot{\mathbf{U}}_{link,n+m}^I = \mathbf{F}_{link,n+m}^I \quad (64b)$$

where $\tilde{\mathbf{M}}^I$ is defined by:

$$\tilde{\mathbf{M}}^I = \mathbf{M}^I + \Delta T \gamma_I \mathbf{C}^I + \Delta T^2 \beta_I \mathbf{K}^I \quad (65)$$

γ_I and β_I being the Newmark parameters in the implicit sub-domain. Here we use $\gamma_I = \frac{1}{2}$ and $\beta_I = \frac{1}{4}$.

Remark The forces \mathbf{F}_D^I due to Dirichlet conditions are not taken into account in the free equilibrium equation (64a) because $\Gamma_G \cap \Gamma_D^I = \emptyset$.

In the explicit sub-domain Ω_E , using the CD-Lagrange time integrator presented in Sect. 2.3, the velocity (44b) can be decomposed into a free part and a link part as follows:

$$\dot{\mathbf{U}}_{free,n+j}^E = \dot{\mathbf{U}}_{n+j-1}^E + \frac{1}{2}\mathbf{W}_{n+j-1}^E + \frac{1}{2}\mathbf{W}_{free,n+j}^E \quad (66a)$$

$$\dot{\mathbf{U}}_{link,n+j}^E = \frac{1}{2}\mathbf{W}_{link,n+j}^E \quad (66b)$$

In an analogous manner, the decomposition of the displacement (44a) gives the two equations:

$$\mathbf{U}_{free,n+j}^E = \mathbf{U}_{n+j-1}^E + \Delta t \dot{\mathbf{U}}_{n+j-1}^E + \frac{\Delta t}{2}\mathbf{W}_{n+j-1}^E \quad (67a)$$

$$\mathbf{U}_{link,n+j}^E = 0 \quad (67b)$$

It can be remarked that the link part of the displacement is zero because we know the configuration at the beginning of the micro-time step as classically done in explicit computation. Thus the configuration given by Eq. (67a) has not to be corrected.

We can decompose the Eq. (55) into two equations related to free and link quantities:

$$\mathbf{M}_{lump}^E \dot{\mathbf{U}}_{free,n+j+\frac{1}{2}}^E = \mathbf{M}_{lump}^E \dot{\mathbf{U}}_{free,n+j-\frac{1}{2}}^E + \Delta t \left(\mathbf{F}_{ext,n+j}^E - \mathbf{F}_{int,n+j}^E - \mathbf{C} \dot{\mathbf{U}}_{n+j-\frac{1}{2}}^E \right) \quad (68a)$$

$$\mathbf{M}_{lump}^E \dot{\mathbf{U}}_{link,n+j+\frac{1}{2}}^E = \mathbf{M}_{lump}^E \dot{\mathbf{U}}_{link,n+j-\frac{1}{2}}^E + \Delta t \mathbf{F}_{link,n+j}^E \quad (68b)$$

Remark \mathbf{F}_D^E due to Dirichlet conditions and contact/impact impulses \mathbf{I}^E are not taken into account in the free equilibrium equation (68a) because $\Gamma_G \cap \Gamma_D^E = \emptyset$ and $\Gamma_G \cap \Gamma_C^E = \emptyset$.

Using the decomposition given in (60a) and (60b), the interface equation (59) becomes:

$$\mathbf{L}_G^E \dot{\mathbf{U}}_{link,n+j}^E + \mathbf{L}_G^I \dot{\mathbf{U}}_{link,n+j}^I = -\mathbf{L}_G^E \dot{\mathbf{U}}_{free,n+j}^E - \mathbf{L}_G^I \dot{\mathbf{U}}_{free,n+j}^I \quad (69)$$

Substituting (61b), (64b), (66b) and (68b) into (69) gives:

$$\begin{aligned} & \frac{\Delta t}{2} \mathbf{L}_G^E (\mathbf{M}_{lump}^E)^{-1} \mathbf{F}_{link,n+j}^E + \Delta T \gamma_I \mathbf{L}_G^I (\tilde{\mathbf{M}}^I)^{-1} \mathbf{F}_{link,n+j}^I \\ & = -\mathbf{L}_G^E \dot{\mathbf{U}}_{free,n+j}^E - \mathbf{L}_G^I \dot{\mathbf{U}}_{free,n+j}^I \end{aligned} \quad (70)$$

Using the relation $\mathbf{F}_{link}^k = (\mathbf{L}_G^k)^T \boldsymbol{\Lambda}_G$, the interface equation to be solved can be written as follows:

$$(\mathbf{H}^E + \mathbf{H}^I) \boldsymbol{\Lambda}_{G,n+j} = -\mathbf{L}_G^E \dot{\mathbf{U}}_{free,n+j}^E - \mathbf{L}_G^I \dot{\mathbf{U}}_{free,n+j}^I \quad (71)$$

where:

$$\mathbf{H}^E = \frac{\Delta t}{2} \mathbf{L}_G^E (\mathbf{M}_{lump}^E)^{-1} (\mathbf{L}_G^E)^T \quad (72)$$

$$\mathbf{H}^I = \Delta T \gamma_I \mathbf{L}_G^I (\tilde{\mathbf{M}}^I)^{-1} (\mathbf{L}_G^I)^T \quad (73)$$

and $\dot{\mathbf{U}}_{free,n+j}^I$ is the linear interpolation of $\dot{\mathbf{U}}_{free,n+m}^I$ at time t_{n+j} such as:

$$\dot{\mathbf{U}}_{free,n+j}^I = \left(1 - \frac{j}{m}\right) \dot{\mathbf{U}}_{free,n}^I + \frac{j}{m} \dot{\mathbf{U}}_{free,n+m}^I \quad (74)$$

A flowchart of the explicit-implicit HATI for contact/impact problems is given in Algorithm 1.

Algorithm 1 Multi-time-scale contact algorithm

1. Initialization
 2. Loop on the coarse time step
 - (a) Solve the free problem (64a) on the implicit sub-domain Ω_I
 - (b) Loop on the fine time step for $0 \leq j \leq m$
 - i. Solve the interface problem (71)
 - ii. Solve the Dirichlet boundary conditions at the fine time scale
 - iii. Solve the contact problem (56) (see ‘‘Appendix 1’’)
 - iv. Solve the constrained problem (55) on the sub-domain Ω_E
 - (c) End loop on the fine time step
 - (d) Solve the constrained problem (54) on the sub-domain Ω_I
 3. End loop on the coarse time step
-

The multi-time-scale method used here is stable. A proof of stability, using the pseudo-energy method [50], can be found in [42]. In practice, when different time scales are used, the ratio m between the two time scales allows to control the possible dissipated energy at the interface between the sub-domains. The discrete energy balance equation for the explicit-implicit HATI is given in ‘‘Appendix 2.2’’.

3 Numerical examples

3.1 Contact/impact of two identical elastic bars

In order to check the accuracy and the efficiency of the proposed explicit contact/impact time-integrator, a one-dimensional contact/impact problem is investigated in this section. Numerical results are computed using the CD-Lagrange time integrator (47) and compared to the numerical results obtained using Moreau-Jean’s time-stepping schemes

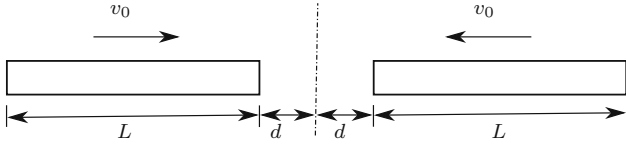


Fig. 3 Configuration of two identical bars in contact

(50) for $\theta = 1$, denoted by Moreau-implicit. Kinematic and dual variables computed by the finite element method are also compared to the analytical results. Numerical energy balance and empirical order of convergence are also discussed. The error indicator used for the convergence study is presented in “Appendix 3”.

This one-dimensional contact/impact problem depicted in Fig. 3 is widely examined in the literature [3, 14, 17, 20, 21, 24–26, 50, 51, 59, 82]. The example consists of two identical linear elastic bars moving with equal speed in opposite directions.

The simulation parameters are given in the following: the elastic modulus $E = 2.110^{11}$ Pa, the density ρ

$= 7847 \text{ kg/m}^3$, the initial length $L = 0.254 \text{ m}$, the section $A = 0.64510^{-3} \text{ m}^2$, the initial gap $d = 0.210^{-3} \text{ m}$ and the initial velocity $v_0 = 5 \text{ ms}^{-1}$. A detailed analytical solution of this example can be found in [20]. The bars are discretized in 40 equal length linear elastic finite elements. The time step used to obtain the numerical solution is chosen as $\Delta t = 0.8 \Delta t_{\text{critical}} \approx 9.810^{-7} \text{ s}$, where $\Delta t_{\text{critical}} \approx 1.2210^{-6} \text{ s}$ is the time step satisfying the CFL condition [30] for stability requirement of the CD explicit time integrator. Figure 4 displays the displacement, the velocity and the contact force of the left bar.

In Fig. 4, the results obtained with the CD-Lagrange algorithm are found to be very accurate compared to the exact solution. During the contact time, a very small contact penetration is observed for both CD-Lagrange and Moreau-implicit schemes, but this penetration gets smaller as the time step size decreases. During the contact, no spurious oscillation is observed contrary to what was observed for instance in [3, 20, 32, 34]. After the contact’s release, local oscillations in the velocity are noticed in the case of the CD-Lagrange

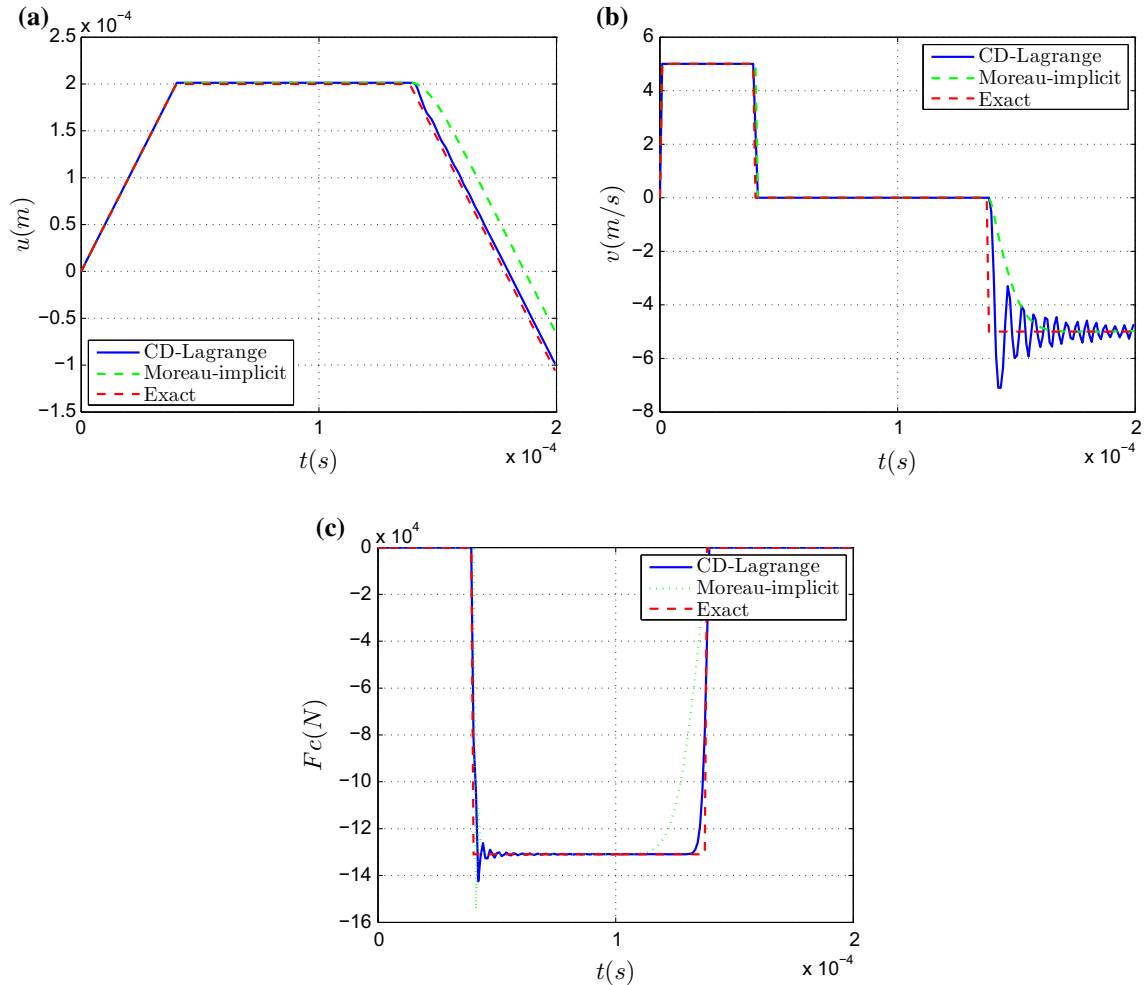


Fig. 4 Contact of two bars: displacement, velocity and contact force of the left bar $\Delta t \approx 9.810^{-7} \text{ s}$

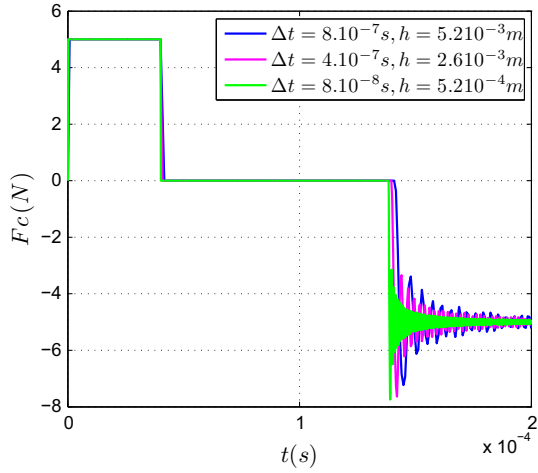


Fig. 5 Contact of two bars: velocity of the left bar for different element lengths h and different time steps Δt

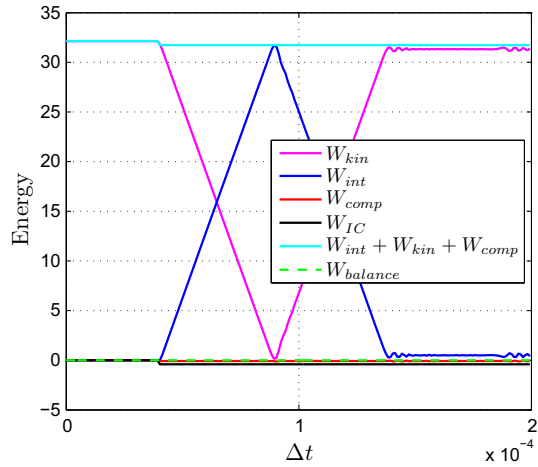


Fig. 6 Contact of two bars: energy balance of the left bar for the CD-Lagrange scheme

scheme. It is mainly due to spurious oscillations well known for the CD time integrator. However, when carried out a space-time refinement, the result converges to the solution as highlighted in Fig. 5.

Figure 6 presents the energy balance of the left bar for the CD-Lagrange scheme. We observe that during the impact, a part of the kinetic energy is converted into internal energy and a loss of kinetic energy is observed. This energy loss (1.25% of the kinetic energy) is due to the jump in the velocity during the impact. The same observation is made for Moreau-Jean's schemes [17,24,25]. After the impact time, no more dissipation is observed because the work done by the contact forces remains equal to zero [4]. It can be remarked that this kinetic energy loss vanishes with a refinement of the mesh around the contact area [20].

Figure 7a displays contact force for different time steps. We observe that the peak corresponding to the first contact between the two bars, increases when the time step decreases. We call this effect an “impact”. However, during the contact period following the time step of the impact, the force becomes independent on the time step. We call this effect a “contact”. As for the contact force, we observe in Fig. 7b that the acceleration converges except for the value corresponding to this first contact between the two bars. Thus, two behaviors are to be distinguished here. The first behavior corresponds to the impact which occurs when the bars come into contact. This instantaneous phenomenon involves a velocity discontinuity. This is why the contact impulse is the key unknown of the problem. The second behavior is a persistent contact which is a smooth phenomenon without any velocity discontinuity. In contrast with the force and the acceleration, we observe in Fig. 8 that the impulse of the impact is independent on the time step. It only depends on the mass of the degrees of freedom involved in the impact. This is why, thanks to the refinement of the mesh, we can

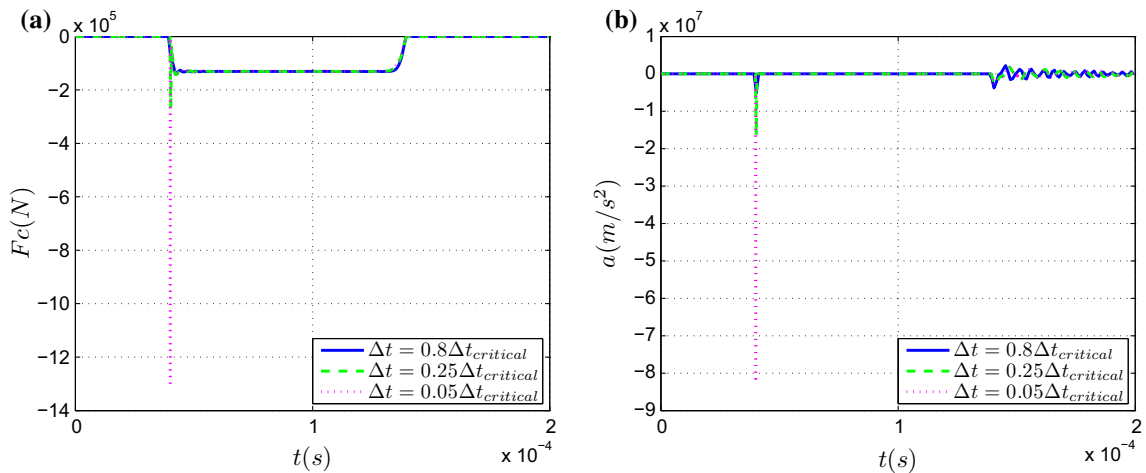


Fig. 7 Contact of two bars: contact force and acceleration of the left bar for different time steps

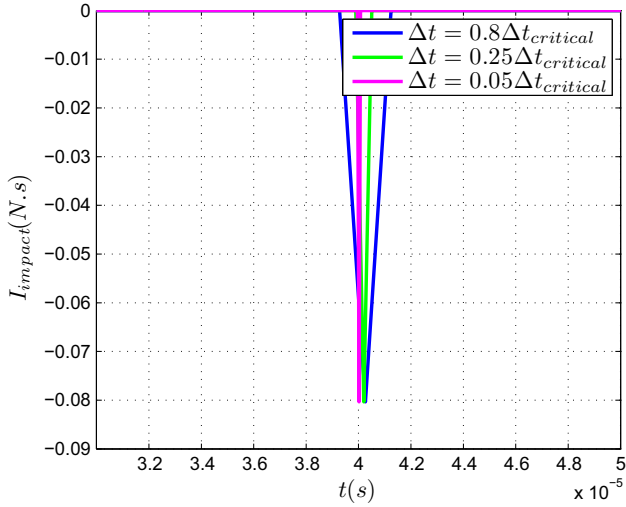


Fig. 8 Contact of two bars: impact impulse of the left bar for different time steps

decrease the impulse and tend to a conservative behavior (no energy dissipation).

For this one dimensional finite element problem, we will study a space-time numerical order of convergence. For this purpose, the size h of the finite elements of the homogeneous mesh is calculated for each time step Δt so as $h = c * \Delta t$, c being the celerity of the elastic wave. Figure 9 presents the global order of convergence in time after contact's release. The Moreau-implicit scheme is of order $\frac{1}{2}$ and the CD-Lagrange time integrator is of order 1 in displacement as shown in Fig. 9a. The same orders are illustrated in Fig. 9b for velocity.

Figure 10 presents the global order of convergence in space after contact's release. As for the global order of convergence in time, the Moreau-implicit scheme is of order $\frac{1}{2}$ and the CD-Lagrange time integrator is of order 1 in displacement and in velocity as shown in Fig. 10.

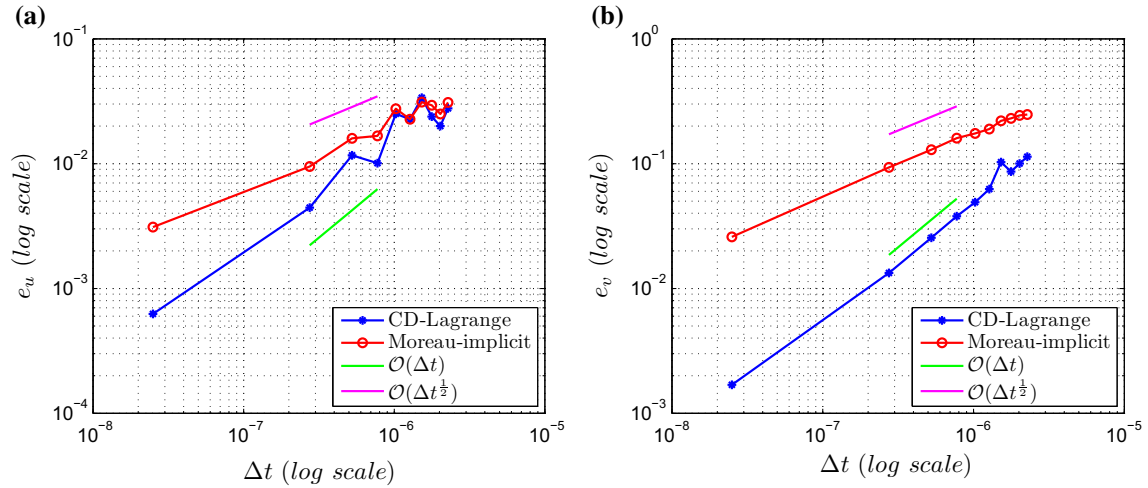


Fig. 9 Contact of two bars: empirical order of convergence in time after contact's release for **a** displacement, **b** velocity

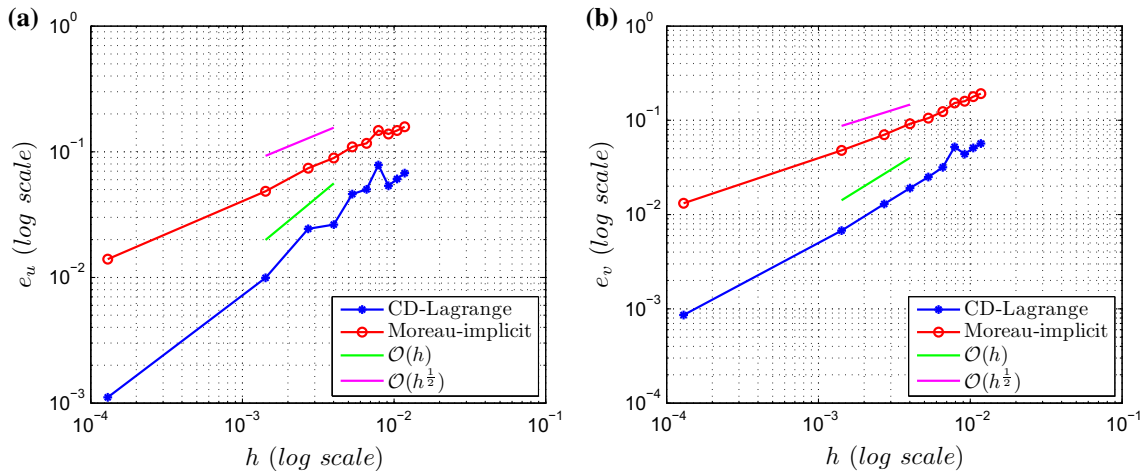


Fig. 10 Contact of two bars: empirical order of convergence in space after contact's release for **a** displacement, **b** velocity

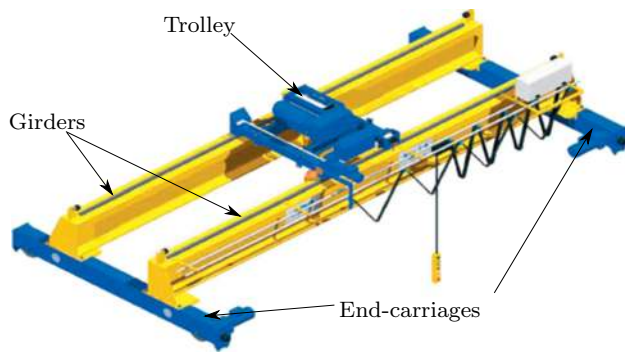


Fig. 11 Example of a bridge crane

The previous results confirm both the space and time convergence of the proposed explicit time integrator for contact/impact dynamics. Furthermore, it is observed that this time integrator has generally a higher order of convergence than Moreau-Jean's schemes, and exhibit a suitable energy behavior.

3.2 Bridge crane under seismic loading

In this section, an industrial example of a bridge crane is carried out using the explicit-implicit HATI algorithm described in Algorithm 1. The numerical results are compared to a full-explicit simulation performed with the CD-Lagrange algorithm developed in Sect. 2.3.

This numerical example consists of a bridge crane subjected to an earthquake. A bridge crane is usually located

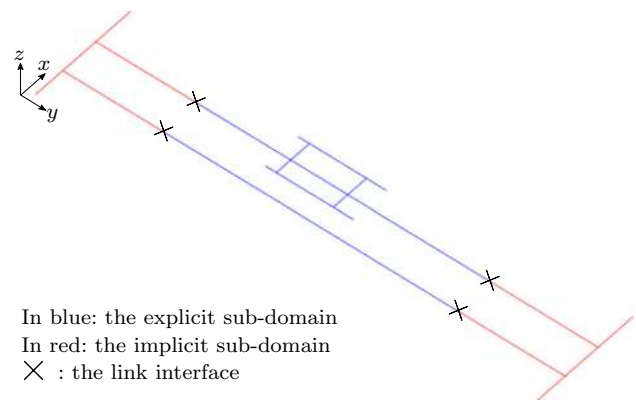


Fig. 13 Bridge crane: sub-domains partition

overhead in buildings or warehouses. It is composed of two girders, two end-carriages and a trolley as shown in Fig. 11. A bridge crane operation is characterized by three main motions: the trolley translational motion on the girders, the long travel motion of the crane on the runway rails and the hoisting motion of the lifted load, driven by the hoist installed on the trolley.

During an earthquake, the bridge crane is exposed to several impacts between trolley wheels and girders, as well as between crane wheels and the runway rails of the building. These several impacts can cause large damage in the bridge crane which can fall on some critical materials in the building. For risk mitigation purpose, the qualification of bridge cranes, with respect to normative seismic design

	Dimensions	Section	Masse
End-carriages			3003 kg
Girders			10844 kg
Trolley			5150 kg

Fig. 12 Bridge crane: geometry, beam sections and masses

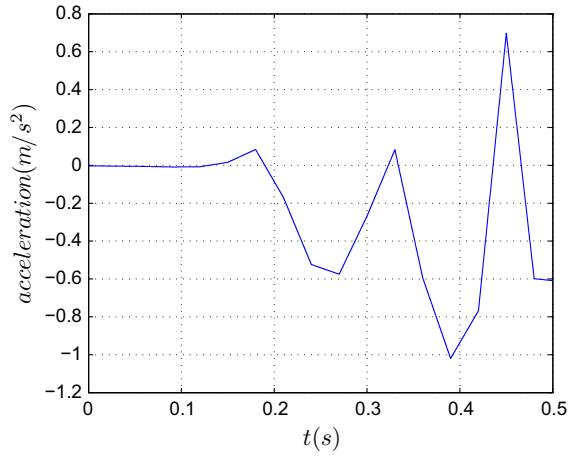


Fig. 14 Bridge crane: acceleration applied to bridge crane in the z direction

requirements, requests for strengthened non-linear simulation techniques, including an adequate modeling of the impact phenomenon.

For both numerical simulations, the bridge crane is modeled using linear elastic beam elements where the elastic modulus is $E = 2.110^{11}$ Pa. The crane wheels are clamped and only the contact between trolley wheels and girders are considered. The model dimensions and masses are given in Fig. 12. The explicit domain is discretized with equal length ($h_{exp} = 100$ mm) finite elements as well as the implicit domain ($h_{imp} = 200$ mm). The fine time step of the explicit domain is $\Delta t \approx 2.8510^{-7}$ s and the coarse time step of the implicit domain is $\Delta T = 100 * \Delta t$. The bridge crane is first subjected to the gravity ($g = 10$ m/s²). The girders and the end-carriages are also subjected to the temporal acceleration depicted in Fig. 14 in the z direction, where this acceleration represents a beginning part of an earthquake signal. For the asynchronous simulation, the partition between explicit and implicit sub-domains is depicted in Fig. 13.

Figures 15 and 16 show, respectively, the displacement and the velocity of one of the four contacts between the trolley and the girders (the same observations can be made for the other contacts).

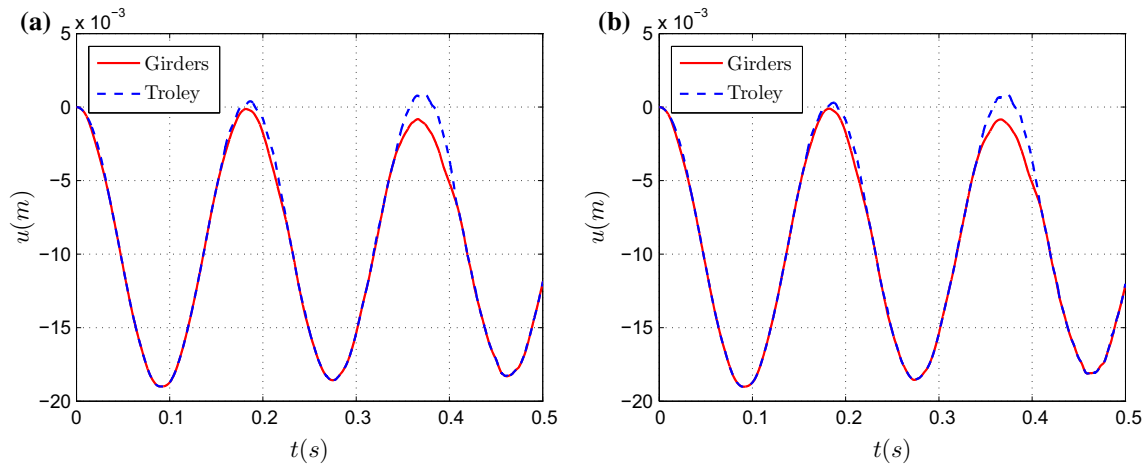


Fig. 15 Bridge crane: displacement of the trolley and the girders **a** full-explicit simulation, **b** asynchronous explicit-implicit simulation

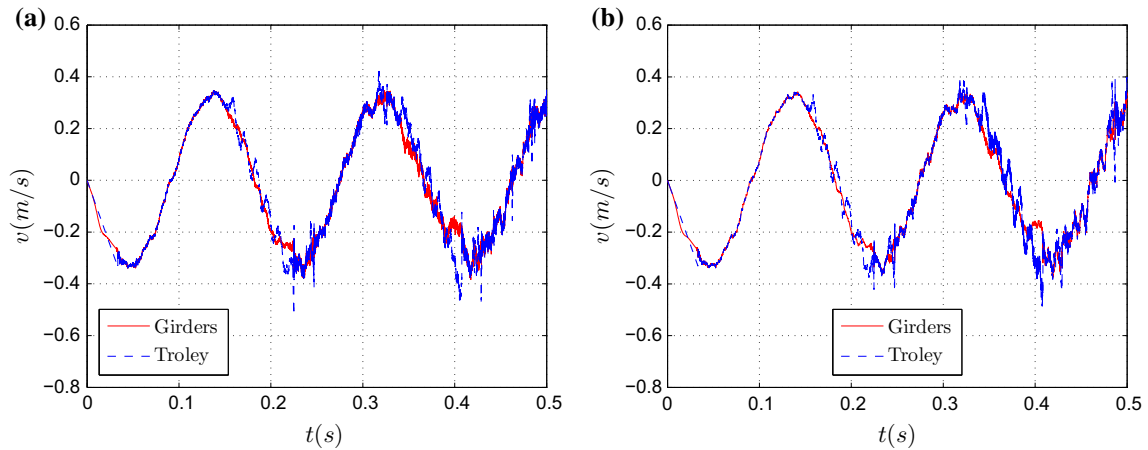


Fig. 16 Bridge crane: velocity of the trolley and the girders **a** full-explicit simulation, **b** asynchronous explicit-implicit simulation

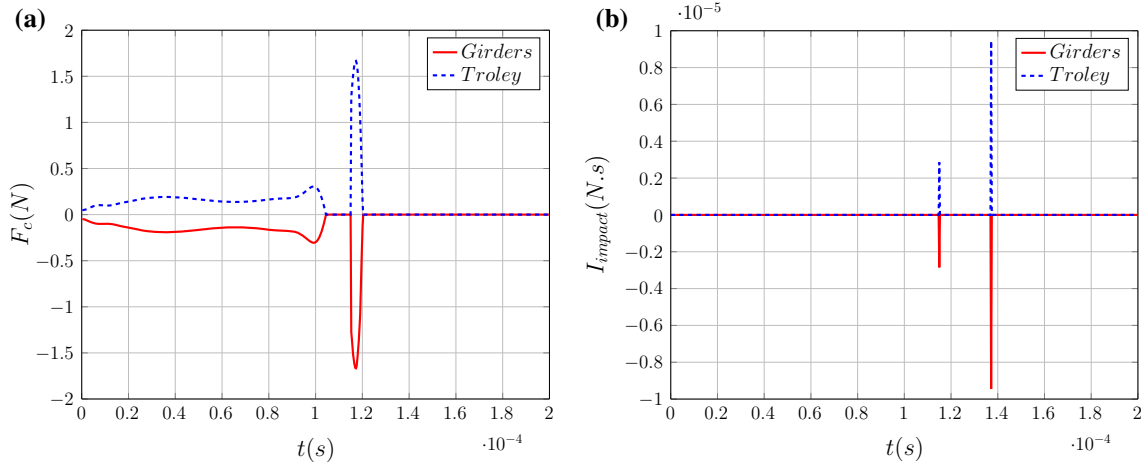


Fig. 17 Bridge crane: contact force and impact impulse, zoom on $t \in [0, 2 \cdot 10^{-4}]$

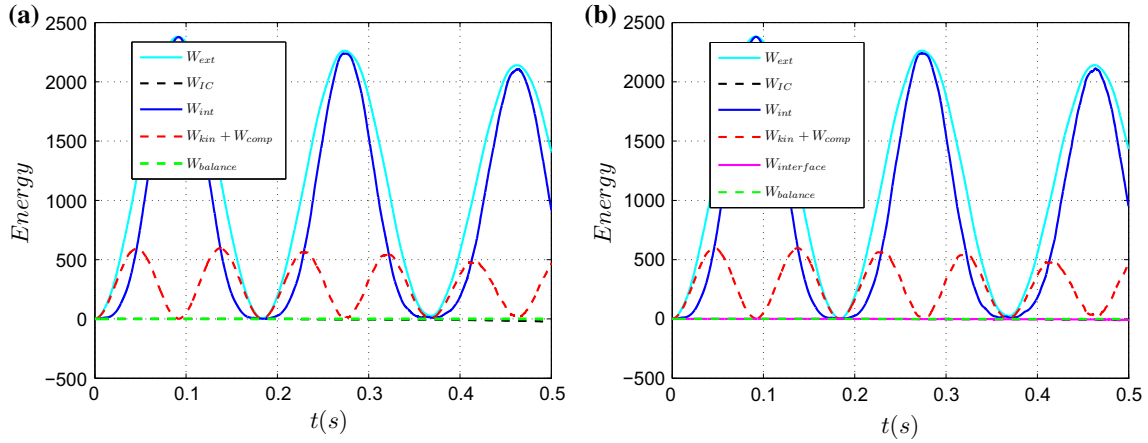


Fig. 18 Bridge crane: discrete energy balance **a** full-explicit simulation, **b** asynchronous explicit-implicit simulation

We note that the asynchronous explicit-implicit and the full explicit simulations give very similar kinematic results. The velocity presents some oscillations which are due to the velocity jumps when impacts occur and to the high frequency modes of the bridge crane. The introduction of a numerical damping would help to damp out these oscillations.

In order to analyse and distinguish the contact and impact phases, Fig. 17 presents a zoom on $t \in [0, 2 \cdot 10^{-4}]$ of the contact force and the impact impulse. We recall that an impact is a transition from a non contact state to a contact state (see the bars example previously discussed).

From Fig. 17a, we can see that the trolley and the girders are initially in contact. The first bounce of the trolley is observed at $t \approx 1.05 \cdot 10^{-4}$ s. When the trolley comes into contact again with the girders, an impact occurs at $t \approx 1.18 \cdot 10^{-4}$ s as we can see in Fig. 17b. This impact is followed by a contact phase before the trolley bounces again at $t \approx 1.2 \cdot 10^{-4}$ s. Figure 17b shows that a second impact occurs at $t \approx 1.38 \cdot 10^{-4}$ s but it is not followed by a contact phase.

This analysis shows that the bridge crane under seismic loading is subjected to several impacts followed, sometimes, by contact phase.

Figure 18 shows that the energy balance equation is conserved for both simulations. The energy dissipated at the interface between implicit and explicit domains remains negligible (see Fig. 19) in comparison to global energies involved in the simulation.

In this example, an asynchronous explicit-implicit time integrator is used for contact/impact dynamic simulation with a ratio of time scales of 100. The results are similar to a full-explicit simulation and the energy dissipated at the explicit-implicit interface remains very low. The gain in the computational time is not significant (23 min for a full-explicit simulation and 20 min for the explicit-implicit simulation). However, a higher ratio of time scales and an adequate domain decomposition (small explicit sub-domain) should be considered for achieving substantial gains in terms of computation time.

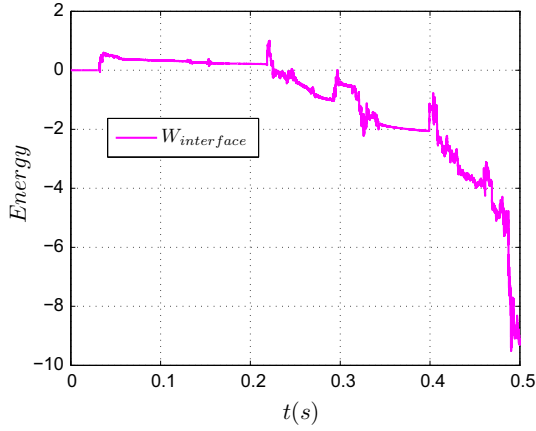


Fig. 19 Bridge crane: energy dissipated at the explicit–implicit interface

The feasibility of the asynchronous explicit–implicit approach has been proven and its interest for an industrial application has been highlighted [23]. Further studies are in progress to estimate the CPU gain when the bridge crane is modeled using a full 3D FEM.

4 Conclusions

This work has led to the development of an explicit–implicit HATI for contact/impact dynamics. This method allows us to adopt an explicit contact/impact time integrator in the contact area and an implicit time integrator with a coarse mesh in the rest of the domain. The time integrator is tested on a bridge crane under seismic loading, and gives accurate numerical results along with a very satisfactory energy behavior. Work is in progress to extend this approach to a full 3D model for the bridge crane.

A Lagrange explicit time-stepping contact/impact time integrator has been also proposed. The main advantages of this time integrator are: no detection of events, no iteration to solve the equilibrium equation and the contact constraints, and no additional numerical parameters. The algorithm, tested on an academic example and compared to Moreau-Jean’s schemes, turned out to be accurate. Indeed, the proposed scheme has generally a higher numerical order of convergence than the implicit Moreau-Jean scheme ($\theta = 1$).

Acknowledgements We acknowledge the French technical center of mechanical industry (CETIM) for its partnership in this project initiated by the French crane industry.

Appendix 1: CD-Lagrange contact/impact algorithm

The implementation of the time integrator (47) is illustrated in the following flow-chart (Algorithm 2). For sake of sim-

plicity, no contact searching procedure is used here, as we assume the p prospective contact points to be known. Thus, the $(p \times n)$ boolean contact operator \mathbf{L}_c is known at the beginning of the computation, where n is the number of DOFs of the problem. In this paper, this algorithm will be called CD-Lagrange time integrator.

Algorithm 2 Lagrange explicit contact/impact algorithm

Input $\mathbf{X}_0, \mathbf{U}_0, \dot{\mathbf{U}}_0, \Delta t, e$

1: Initialize $\dot{\mathbf{U}}_0, \dot{\mathbf{U}}_{\frac{1}{2}}$

2: $t \leftarrow 0$

3: **while** ($t \leq t_{final}$) **do**

4: $t \leftarrow t + \Delta t$

5: Compute $\mathbf{U}_{n+1}, \mathbf{g}_{N,n+1}$ ▷ (44a), (47b)

6: $\lambda_{c,n+\frac{3}{2}} \leftarrow 0$

7: **for all** ($l \leq p$) **do** ▷ Loop on all prospective contact points

8: **if** ($g_N^l \leq 0$) **then**

9: $v_{n+\frac{3}{2}}^l \leftarrow 0$

10: Compute $\lambda_{c,n+\frac{3}{2}}^l$ ▷ (48)

11: **if** ($\lambda_{c,n+\frac{3}{2}}^l < 0$) **then**

12: $\lambda_{c,n+\frac{3}{2}}^l \leftarrow 0$

13: **end if**

14: **end if**

15: **end for**

16: Compute $\mathbf{I}_{n+1}, \mathbf{W}_{n+1}$ ▷ (47f), (47c)

17: Compute $\dot{\mathbf{U}}_{n+\frac{3}{2}}, \mathbf{v}_{c,n+\frac{3}{2}}$ ▷ (47d), (47e)

Output if impact: $\mathbf{U}_{n+1}, \mathbf{I}_{n+1}, \dot{\mathbf{U}}_{n+1}$ ▷ (44b)

Output if contact: $\mathbf{U}_{n+1}, \mathbf{I}_{n+1}, \dot{\mathbf{U}}_{n+1}, \mathbf{F}_{c,n+1}, \dot{\mathbf{U}}_{n+1}$ ▷ (44b), (45), (46)

18: **end while**

Appendix 2: Discrete energy balance equation

Appendix 2.1: Explicit CD-Lagrange time integrator for contact/impact problems

In order to evaluate the energy properties of the proposed CD-Lagrange time integrator, we give the following discrete energy balance equation. It is obtained by multiplying the nonsmooth equation of motion (32) by $\dot{\mathbf{U}}^T$.

$$d \left(\frac{1}{2} \dot{\mathbf{U}}^T \mathbf{M} \dot{\mathbf{U}} \right) = \dot{\mathbf{U}}^T \mathbf{F} dt + \dot{\mathbf{U}}^T d\mathbf{I} \quad (75)$$

where (assuming that $\mathbf{C} = 0$ for sake of simplicity):

$$\mathbf{F} = \mathbf{F}_{ext} - \mathbf{F}_{int} \quad (76)$$

Using the relation $d\mathbf{U} = \dot{\mathbf{U}} dt$, we get the following energy balance:

$$d\left(\frac{1}{2}\dot{\mathbf{U}}^T \mathbf{M}\dot{\mathbf{U}}\right) = d\mathbf{U}^T \mathbf{F} + \dot{\mathbf{U}}^T d\mathbf{I} \quad (77)$$

The term in the parenthesis on the left hand side is the kinetic energy, and the two terms on the right hand side are the rate of internal/external work and the contact/impact impulse work. The discrete form of the energy balance equation is obtained by expressing the increment of the kinetic energy over the time interval $[t_n, t_{n+1}]$:

$$\left[\frac{1}{2}\dot{\mathbf{U}}^T \mathbf{M}\dot{\mathbf{U}}\right]_n^{n+1} = \langle \dot{\mathbf{U}}_n \rangle^T \mathbf{M}[\dot{\mathbf{U}}_n] \quad (78)$$

The notations $[\cdot]$ and $\langle \cdot \rangle$ denote the increment and the mean value. They are defined as follows:

$$[X_n] = (X_{n+1} - X_n) \quad (79)$$

$$\langle X_n \rangle = \frac{1}{2}(X_{n+1} + X_n) \quad (80)$$

The path independent kinetic energy increment uses the expressions of means value $\langle \cdot \rangle$ and increment $[\cdot]$ (see Eq. (78)). For the CD time integrator, from Eq. (44a) and (44b), we obtain the following expressions in terms of mean values and increments:

$$[\dot{\mathbf{U}}_n] = \langle \mathbf{W}_n \rangle \quad (81a)$$

$$[\mathbf{U}_n] = \Delta t \langle \dot{\mathbf{U}}_n \rangle - \frac{\Delta t}{4}[\mathbf{W}_n] \quad (81b)$$

Combining (78) and (81a) involves:

$$\left[\frac{1}{2}\dot{\mathbf{U}}^T \mathbf{M}\dot{\mathbf{U}}\right]_n^{n+1} = \Delta t \langle \dot{\mathbf{U}}_n \rangle^T \langle \mathbf{F}_n \rangle + \langle \dot{\mathbf{U}}_n \rangle^T \langle \mathbf{I}_n \rangle \quad (82)$$

From (81b) we obtain:

$$\begin{aligned} \left[\frac{1}{2}\dot{\mathbf{U}}^T \mathbf{M}\dot{\mathbf{U}}\right]_n^{n+1} &= [\mathbf{U}_n]^T \langle \mathbf{F}_n \rangle + \frac{\Delta t}{4}[\mathbf{W}_n]^T \langle \mathbf{F}_n \rangle + \frac{[\mathbf{U}_n]^T}{\Delta t} \langle \mathbf{I}_n \rangle + \frac{1}{4}[\mathbf{W}_n]^T \langle \mathbf{I}_n \rangle \\ &= [\mathbf{U}_n]^T \langle \mathbf{F}_n \rangle + \frac{[\mathbf{U}_n]^T}{\Delta t} \langle \mathbf{I}_n \rangle + \frac{1}{4}[\mathbf{W}_n]^T (\Delta t \langle \mathbf{F}_n \rangle + \langle \mathbf{I}_n \rangle) \\ &= [\mathbf{U}_n]^T \langle \mathbf{F}_n \rangle + \frac{[\mathbf{U}_n]^T}{\Delta t} \langle \mathbf{I}_n \rangle + \frac{1}{4}[\mathbf{W}_n]^T M \langle \mathbf{W}_n \rangle \end{aligned} \quad (83)$$

Then, the discretized energy balance can be written as follows:

$$\left[\frac{1}{2}\dot{\mathbf{U}}^T \mathbf{M}\dot{\mathbf{U}} - \frac{1}{8}\mathbf{W}^T \mathbf{M}\mathbf{W}\right]_n^{n+1} = [\mathbf{U}_n]^T \langle \mathbf{F}_n \rangle + \frac{[\mathbf{U}_n]^T}{\Delta t} \langle \mathbf{I}_n \rangle \quad (84)$$

which can also be denoted:

$$\Delta W_{kin,n+1} + \Delta W_{comp,n+1} + \Delta W_{int,n+1} = \Delta W_{ext,n+1} + \Delta W_{IC,n+1} \quad (85)$$

The expression of energies involved in the above balance energy are:

$$\Delta W_{kin,n+1} = \left[\frac{1}{2}\dot{\mathbf{U}}^T \mathbf{M}\dot{\mathbf{U}}\right]_n^{n+1} \quad (86)$$

$$\Delta W_{comp,n+1} = \left[-\frac{1}{8}\mathbf{W}^T \mathbf{M}\mathbf{W}\right]_n^{n+1} \quad (87)$$

$$\Delta W_{ext,n+1} = [\mathbf{U}_n]^T \langle \mathbf{F}_{ext,n} \rangle \quad (88)$$

$$\Delta W_{int,n+1} = [\mathbf{U}_n]^T \langle \mathbf{F}_{int,n} \rangle \quad (89)$$

$$\Delta W_{IC,n+1} = \frac{[\mathbf{U}_n]^T}{\Delta t} \langle \mathbf{I}_n \rangle \quad (90)$$

and ΔW_{kin} , ΔW_{int} , ΔW_{comp} , ΔW_{ext} , ΔW_{IC} are, respectively, the increments over the time step of the kinetic, internal, complementary, external and impact/contact energies with explicit time integrator.

It can be noticed that the quantities inside bracket on the left hand side are path independent quantities (conservative quantities) (see [50]). The balance energy (85) corresponds to a generalization of the Newmark energy balance given in [57] to the case of contact/impact dynamics.

Appendix 2.2: Explicit–implicit HATI for contact/impact problems

In order to check the energy properties of the proposed explicit–implicit HATI, we recall the discrete energy balance equation between t_0 and t_m :

$$\begin{aligned} \Delta W_{kin,m}^I + \Delta W_{int,m}^I \\ + \sum_{j=1}^m (\Delta W_{kin,j}^E + \Delta W_{int,j}^E + \Delta W_{comp,j}^E) = \Delta W_{ext,m}^I \quad (91) \\ + \Delta W_{D,m}^I + \sum_{j=1}^m (\Delta W_{ext,j}^E + \Delta W_{IC,j}^E + \Delta W_{D,j}^E) \\ + \Delta W_{interface} \end{aligned}$$

The expressions of the increments over a time step of the kinetic ΔW_{kin} , internal ΔW_{int} , complementary ΔW_{comp} , external ΔW_{ext} and impact/contact ΔW_{IC} energies are given, respectively, in Eqs. (86), (89), (87), (88) and (90). In addition, the definitions of the additional energy terms are given below:

$$\Delta W_{D,e}^k = [\mathbf{U}_e^k]^T \langle \mathbf{F}_{D,e}^k \rangle; \quad e = 0, (j-1); \quad k = I, E \quad (92)$$

$$\Delta W_{interface} = [\mathbf{U}_0^I]^T (L_G^I)^T [\mathbf{A}_{G,0}] + \sum_{j=0}^{m-1} [\mathbf{U}_j^E]^T (L_G^E)^T [\mathbf{A}_{G,j}] \quad (93)$$

Appendix 3: Time error indicator

In contact dynamics, due to velocity discontinuities, the convergence cannot be observed using uniform norm as demonstrated in [2]. For this reason, Moreau [69] introduced the convergence in the sense of filled-in-graph using the Hausdorff distance to measure the error with respect to a reference solution. It is shown in [2] that an equivalent absolute l_1 -norm gives the same order of convergence as the Hausdorff norm and can be used thanks to its easy implementation. For this purpose, we introduce the relative error indicator as follows:

$$e_f = \frac{\Delta t \sum_{i=1}^N |f_i - f(t_i)|}{\Delta t \sum_{i=1}^N |f(t_i)|} = \frac{\sum_{i=1}^N |f_i - f(t_i)|}{\sum_{i=1}^N |f(t_i)|} \quad (94)$$

where N is the number of time steps in the time interval $[0, T]$, f_i the numerical results and $f(t_i)$ is the reference results at time t_i . f indicates generalized coordinate, displacement or velocity.

References

1. Abadie M (2000) Dynamic simulation of rigid bodies: modelling of frictional contact. In: Impacts in mechanical systems, pp 61–144. Springer
2. Acary V (2012) Higher order event capturing time-stepping schemes for nonsmooth multibody systems with unilateral constraints and impacts. *Appl Numer Math* 62(10):1259–1275
3. Acary V (2013) Projected event-capturing time-stepping schemes for nonsmooth mechanical systems with unilateral contact and Coulomb's friction. *Comput Methods Appl Mech Eng* 256:224–250
4. Acary V (2016) Energy conservation and dissipation properties of time-integration methods for nonsmooth elastodynamics with contact. *ZAMM J Appl Math Mech* 96:585–603
5. Acary V, Brogliato B (2008) Numerical methods for nonsmooth dynamical systems: applications in mechanics and electronics, vol 35. Springer, Berlin
6. Acary V, Jean M (2000) Numerical modeling of three dimensional divided structures by the non smooth contact dynamics method: application to masonry structures. In: The fifth international conference on computational structures technology, pp 211–221
7. Alart P, Curnier A (1991) A mixed formulation for frictional contact problems prone to Newton like solution methods. *Comput Methods Appl Mech Eng* 92(3):353–375
8. Anitescu M, Potra FA, Stewart DE (1999) Time-stepping for three-dimensional rigid body dynamics. *Comput Methods Appl Mech Eng* 177(3):183–197
9. Armero F, Petőcz E (1998) Formulation and analysis of conserving algorithms for frictionless dynamic contact/impact problems. *Comput Methods Appl Mech Eng* 158(3):269–300
10. Baraff D (1994) Fast contact force computation for nonpenetrating rigid bodies. In: Proceedings of the 21st annual conference on computer graphics and interactive techniques, pp 23–34. ACM, New York, USA
11. Belytschko T, Liu W, Moran B (2000) Nonlinear finite elements for continua and structures. Wiley, New York
12. Belytschko T, Mullen R (1976) Mesh partitions of explicit–implicit time integration. In: Formulations and computational algorithms in finite element analysis, pp 673–690
13. Belytschko T, Mullen R (1978) Stability of explicit–implicit mesh partitions in time integration. *Int J Numer Methods Eng* 12(10):1575–1586
14. Belytschko T, Neal M (1991) Contact-impact by the pinball algorithm with penalty and Lagrangian methods. *Int J Numer Methods Eng* 31:547–572
15. Betsch P, Steinmann P (2001) Conservation properties of a time fe methodpart ii: time-stepping schemes for non-linear elastodynamics. *Int J Numer Methods Eng* 50(8):1931–1955
16. Brogliato B, Ten Dam A, Paoli L, Genot F, Abadie M (2002) Numerical simulation of finite dimensional multibody nonsmooth mechanical systems. *Appl Mech Rev* 55(2):107–150
17. Brüls O, Acary V, Cardona A (2014) Simultaneous enforcement of constraints at position and velocity levels in the nonsmooth generalized- α scheme. *Comput Methods Appl Mech Eng* 281:131–161
18. Brun M, Batti A, Limam A, Combescure A (2012) Implicit/explicit multi-time step co-computations for predicting reinforced concrete structure response under earthquake loading. *Soil Dyn Earthq Eng* 33(1):19–37
19. Brun M, Batti A, Limam A, Gravouil A (2012) Explicit/implicit multi-time step co-computations for blast analyses on a reinforced concrete frame structure. *Finite Elem Anal Des* 52:41–59
20. Carpenter NJ, Taylor RL, Katona MG (1991) Lagrange constraints for transient finite element surface contact. *Int J Numer Methods Eng* 32(1):103–128
21. Casadei F (2002) A hierarchic pinball method for contact-impact in fast transient dynamics. In: VI Congresso Nazionale della Società Italiana di Matematica Applicata e Industriale (SIMAI 2002), Chia (Cagliari), Italy, pp 27–31
22. Chabrand P, Dubois F, Raous M (1998) Various numerical methods for solving unilateral contact problems with friction. *Math Comput Model* 28(4):97–108
23. Chantrait T, Rannou J, Gravouil A (2014) Low intrusive coupling of implicit and explicit time integration schemes for structural dynamics: Application to low energy impacts on composite structures. *Finite Elem Anal Des* 86:23–33
24. Chen QZ, Acary V, Virlez G, Brüls O (2012) A Newmark-type integrator for flexible systems considering nonsmooth unilateral constraints. In: Eberhard P (ed) IMSD 2012—2nd joint international conference on multibody system dynamics. Stuttgart, Germany
25. Chen QZ, Acary V, Virlez G, Brüls O (2013) A nonsmooth generalized- α scheme for flexible multibody systems with unilateral constraints. *Int J Numer Methods Eng* 96(8):487–511
26. Cirak F, West M (2005) Decomposition contact response (dcr) for explicit finite element dynamics. *Int J Numer Methods Eng* 64(8):1078–1110
27. Combescure A, Gravouil A (2001) A time-space multi-scale algorithm for transient structural nonlinear problems. *Méc Ind* 2(1):43–55
28. Combescure A, Gravouil A (2002) A numerical scheme to couple subdomains with different time-steps for predominantly linear transient analysis. *Comput Methods Appl Mech Eng* 191(11):1129–1157
29. Combescure A, Gravouil A, Herry B (2003) An algorithm to solve transient structural non-linear problems for non-matching time-space domains. *Comput Struct* 81(12):1211–1222

30. Courant R, Friedrichs K, Lewy H (1928) Über die partiellen differenzgleichungen der mathematischen physik. *Math Ann* 100(1):32–74
31. Curnier A (1999) Unilateral contact. In: *New developments in contact problems*, pp 1–54. Springer, Wien
32. Dabaghi F, Petrov A, Pousin J, Renard Y (2014) Convergence of mass redistribution method for the one-dimensional wave equation with a unilateral constraint at the boundary. *ESAIM Math Model Numer Anal* 48(4):1147–1169
33. De Saxcé G, Feng ZQ (1998) The bipotential method: a constructive approach to design the complete contact law with friction and improved numerical algorithms. *Math Comput Model* 28(4):225–245
34. Deuffhard P, Krause R, Ertel S (2008) A contact-stabilized newmark method for dynamical contact problems. *Int J Numer Methods Eng* 73(9):1274–1290
35. Dostál Z, Kozubek T, Vlach O, Brzobohatý T (2015) Reorthogonalization-based stiffness preconditioning in feti algorithms with applications to variational inequalities. *Numer Linear Algebra Appl* 22(6):987–998
36. Erickson D, Weber M, Sharf I (2003) Contact stiffness and damping estimation for robotic systems. *Int J Robot Res* 22(1):41–57
37. Faucher V, Combescure A (2003) A time and space mortar method for coupling linear modal subdomains and non-linear subdomains in explicit structural dynamics. *Comput Methods Appl Mech Eng* 192(5):509–533
38. Feng ZQ, Joli P, Cros JM, Magnain B (2005) The bi-potential method applied to the modeling of dynamic problems with friction. *Comput Mech* 36(5):375–383
39. Fetecau R, Marsden JE, West M (2003) Variational multisymplectic formulations of nonsmooth continuum mechanics. In: *Perspectives and problems in nonlinear science*, pp 229–261. Springer
40. Fetecau RC, Marsden JE, Ortiz M, West M (2003) Nonsmooth Lagrangian mechanics and variational collision integrators. *SIAM J Appl Dyn Syst* 2(3):381–416
41. Géradin M, Rixen DJ (2014) *Mechanical vibrations: theory and application to structural dynamics*. Wiley, New York
42. Gravouil A, Combescure A (2001) Multi-time-step explicit-implicit method for non-linear structural dynamics. *Int J Numer Methods Eng* 50(1):199–225
43. Gravouil A, Combescure A (2003) Multi-time-step and two-scale domain decomposition method for non-linear structural dynamics. *Int J Numer Methods Eng* 58(10):1545–1569
44. Gravouil A, Combescure A, Brun M (2015) Heterogeneous asynchronous time integrators for computational structural dynamics. *Int J Numer Methods Eng* 102(3–4):202–232
45. Har J, Tamma K (2012) *Advances in computational dynamics of particles, materials and structures*. Wiley, Singapore
46. Harmon D, Vouga E, Smith B, Tamstorf R, Grinspun E (2009) Asynchronous contact mechanics. *ACM Trans Graph* 28(3):87:1–87:12
47. Hesck C, Betsch P (2009) A mortar method for energy-momentum conserving schemes in frictionless dynamic contact problems. *Int J Numer Methods Eng* 77(10):1468–1500
48. Hesck C, Betsch P (2011) Transient 3d contact problems method: mixed methods and conserving integration. *Comput Mech* 48(4):437–449
49. Hesck C, Betsch P (2011) Transient three-dimensional contact problems: mortar method. Mixed methods and conserving integration. *Comput Mech* 48(4):461–475
50. Hughes TJ (2012) *The finite element method: linear static and dynamic finite element analysis*. Courier Corporation, Kendallville
51. Hughes TJ, Taylor RL, Sackman JL, Curnier A, Kanokkulchai W (1976) A finite element method for a class of contact-impact problems. *Comput Methods Appl Mech Eng* 8(3):249–276
52. Jean M (1999) The non-smooth contact dynamics method. *Comput Methods Appl Mech Eng* 177(3):235–257
53. Jourdan F, Alart P, Jean M (1998) A Gauss–Seidel like algorithm to solve frictional contact problems. *Comput Methods Appl Mech Eng* 155(1):31–47
54. Kane C, Marsden J, Ortiz M, West M (2000) Variational integrators and the Newmark algorithm for conservative and dissipative mechanical systems. *Int J Numer Methods Eng* 49:1295–1325
55. Kikuchi N, Oden JT (1988) *Contact problems in elasticity: a study of variational inequalities and finite element methods*. SIAM, Philadelphia
56. Konyukhov A, Schweizerhof K (2015) On some aspects for contact with rigid surfaces: surface-to-rigid surface and curves-to-rigid surface algorithms. *Comput Methods Appl Mech Eng* 283:74–105
57. Krenk S (2006) Energy conservation in Newmark based time integration algorithms. *Comput Methods Appl Mech Eng* 195(44):6110–6124
58. Laursen T, Chawla V (1997) Design of energy conserving algorithms for frictionless dynamic contact problems. *Int J Numer Methods Eng* 40(5):863–886
59. Laursen TA (2002) *Computational contact and impact mechanics: fundamentals of modeling interfacial phenomena in nonlinear finite element analysis*. Springer, Berlin
60. Leine RI, Aeberhard U, Glocker C (2009) Hamiltons principle as variational inequality for mechanical systems with impact. *J Nonlinear Sci* 19(6):633–664
61. Lemaitre J, Chaboche JL, Benallal A, Desmorat R (2009) *Mécanique des Matériaux Solides–3ème édition*. Dunod
62. Lew A, Marsden J, Ortiz M, West M (2004) Variational time integrators. *Int J Numer Methods Eng* 60(1):153–212
63. Litéwka P (2015) Frictional beam-to-beam multiple-point contact finite element. *Comput Mech* 56(2):243–264
64. Mahjoubi N (2010) *Méthode générale de couplage de schéma d’intégration multiéchelle en temps en dynamique des structures*. Ph.D. thesis, Institut National des Sciences Appliquées de Lyon
65. Mahjoubi N, Gravouil A, Combescure A, Greffet N (2011) A monolithic energy conserving method to couple heterogeneous time integrators with incompatible time steps in structural dynamics. *Comput Methods Appl Mech Eng* 200(9):1069–1086
66. Mahjoubi N, Krenk S (2010) Multi-time-step domain coupling method with energy control. *Int J Numer Methods Eng* 83(13):1700–1718
67. Marsden JE, West M (2001) Discrete mechanics and variational integrators. *Acta Numer* 2001(10):357–514
68. Meier C, Wall WA, Popp A (2017) A unified approach for beam-to-beam contact. *Comput Methods Appl Mech Eng* 315:972–1010
69. Moreau JJ (1978) Approximation en graphe d’une évolution discontinue. *RAIRO Anal Numer* 12(1):75–84
70. Moreau JJ (1988) Unilateral contact and dry friction in finite freedom dynamics. In: *Nonsmooth mechanics and applications*, pp 1–82. Springer, Wien
71. Moreau JJ (1999) Numerical aspects of the sweeping process. *Comput Methods Appl Mech Eng* 177(3):329–349
72. Moreau JJ (2003) Modélisation et simulation de matériaux granulaires. In: *Actes du 35ème Congrès National d’Analyse Numérique*
73. Neto AG, Pimenta PM, Wriggers P (2016) A master-surface to master-surface formulation for beam to beam contact. Part I: frictionless interaction. *Comput Methods Appl Mech Eng* 303:400–429
74. Raous M (1999) Quasistatic Signorini problem with Coulomb friction and coupling to adhesion. In: *New developments in contact problems*, pp 101–178. Springer, Wien
75. Ryckman RA, Lew AJ (2012) An explicit asynchronous contact algorithm for elastic body-rigid wall interaction. *Int J Numer Methods Eng* 89(7):869–896

76. Schindler T, Acary V (2014) Timestepping schemes for nonsmooth dynamics based on discontinuous Galerkin methods: definition and outlook. *Math Comput Simul* 95:180–199
77. Simo J, Tarnow N (1992) The discrete energy-momentum method. Conserving algorithms for nonlinear elastodynamics. *Zeitschrift für angewandte Mathematik und Physik ZAMP* 43(5):757–792
78. Simo JC, Laursen T (1992) An augmented Lagrangian treatment of contact problems involving friction. *Comput Struct* 42(1):97–116
79. Simo JC, Tarnow N, Wong K (1992) Exact energy-momentum conserving algorithms and symplectic schemes for nonlinear dynamics. *Comput Methods Appl Mech Eng* 100(1):63–116
80. Stewart DE (1997) Existence of solutions to rigid body dynamics and the painlevé paradoxes. *Comptes Rendus de l'Académie des Sciences-Series I-Mathematics* 325(6):689–693
81. Stewart DE (1998) Convergence of a time-stepping scheme for rigid-body dynamics and resolution of painlevé's problem. *Arch Ration Mech Anal* 145(3):215–260
82. Taylor RL, Papadopoulos P (1993) On a finite element method for dynamic contact/impact problems. *Int J Numer Methods Eng* 36(12):2123–2140
83. Wang D, Conti C, Beale D (1999) Interference impact analysis of multibody systems. *J Mech Des* 121(1):128–135
84. Wriggers P (1999) Finite elements for thermomechanical contact and adaptive finite element analysis of contact problems. In: *New developments in contact problems*, pp 179–246. Springer, Wien
85. Wu SC, Yang SM, Haug EJ (1986) Dynamics of mechanical systems with Coulomb friction, stiction, impact and constraint addition-deletion-II Planar systems. *Mech Mach Theory* 21(5):407–416
86. Wu SR (2006) Lumped mass matrix in explicit finite element method for transient dynamics of elasticity. *Comput Methods Appl Mech Eng* 195(44):5983–5994